Contrib Mineral Petrol (2016) 171:11
DOI 10.1007/s00410-015-1225-5

ORIGINAL PAPER

Kyanite/corundum eclogites from the Kaapvaal Craton: subducted troctolites and layered gabbros from the Mid- to Early Archean

Qiao Shu[1,2,3] · Gerhard P. Brey[2] · Heidi E. Hoefer[2] · Zhidan Zhao[1] · D. Graham Pearson[3]

Received: 6 August 2015 / Accepted: 15 December 2015 / Published online: 21 January 2016

Abstract An oceanic crustal origin is the commonly accepted paradigm for mantle-derived eclogites. However, the significance of the aluminous members of the eclogite suite, containing kyanite and corundum, has long been underrated and their role neglected in genetic models of cratonic evolution. Here, we present a geochemical and petrological study of a suite of kyanite- and corundum-bearing eclogites from the Bellsbank kimberlite, S. Africa, which originate from depths between 150 and 200 km. Although clearly of high-pressure provenance, these rocks had a low-pressure cumulative origin with plagioclase and olivine as major cumulate phases. This is shown by the very pronounced positive Eu anomalies, low REE abundances, and $\delta^{18}O$ values lower than the Earth's mantle. Many chemical features are identical to modern-day troctolitic cumulates including a light REE depletion akin to MORB, but there are also distinguishing features in that the eclogites are richer in Na, Fe, and Ni. Two of the eclogites have a minimum age of ~3.2 Ga, defined by the extremely unradiogenic $^{87}Sr/^{86}Sr$ (0.7007) in clinopyroxene. Phase equilibria indicate that the parent melts were formed by partial melting below an Archean volcanic center that generated (alkali-)picritic to high-alumina tholeiitic melts from a mantle whose oxygen fugacity was lower than today. Fractional crystallization produced troctolites with immiscible sulfide melt droplets within the mafic crust. Instability of the mafic crust led to deep subduction and re-equilibration at 4–6 GPa. Phase relationships plus the presence of a sample with appreciable modal corundum but no Eu anomaly suggest that kyanite- and corundum-bearing eclogites may also originate as plagioclase-free, higher pressure cumulates of highly aluminous clinopyroxene, spinel, and olivine. This is consistent with the crystallizing phase assemblage from an olivine tholeiitic to picritic magma deeper in the Archean oceanic crust or uppermost mantle. We postulate that the magmatic and subduction processes driving modern plate tectonics already existed in the Meso- to Early Archean.

Keywords Kyanite/corundum eclogite · Troctolite · Eu anomaly · Oxygen fugacity · Strontium isotope ratio

Communicated by Othmar Müntener.

Electronic supplementary material The online version of this article (doi:10.1007/s00410-015-1225-5) contains supplementary material, which is available to authorized users.

✉ Qiao Shu
shuqiaozhejiang@hotmail.com

[1] State Key Laboratory of Geological Processes and Mineral Resources, and School of Earth Science and Mineral Resources, China University of Geosciences, Beijing 100083, China

[2] Institut für Geowissenschaften, FE Mineralogie, Johann Wolfgang Goethe-Universität Frankfurt, Altenhöferallee 1, 60438 Frankfurt, Germany

[3] Department of Earth and Atmospheric Sciences, University of Alberta, Edmonton, AB, Canada

Introduction

The subcratonic lithospheric mantle underneath Archean crust is a potential site for the storage of the residual products of Hadean to Archean partial melting as well as the fractional crystallization products of some of Earth's earliest melts. Metamorphosed mafic and ultramafic assemblages are brought to the Earth's surface as xenoliths in kimberlites. The eclogites and garnet pyroxenites that belong to this group have experienced a complex history,

as partial melts and as cumulates whose history potentially involves seafloor alteration, subduction, devolatilization, metamorphism, metasomatism, and further partial melting (e.g., Jacob 2004). These processes are expressed as phase changes and modifications of element abundances, element ratios, and isotope compositions. The imprints from multiple processes blur the original nature of these rocks. Many of them are therefore interpreted in broad terms as seafloor-altered basalts and gabbros. Certain geochemical and petrological features, however, allow a more detailed reconstruction. For instance, coesite eclogites from Roberts Victor (Kaapvaal craton) show the presence of positive Eu anomalies in garnets and clinopyroxenes along with disparate $\delta^{18}O$ values well outside the normal mantle range (Jacob et al. 2003). This combination and the close geochemical similarities of these rocks with the plutonic section of the oceanic crust indicates that they were originally gabbroic cumulates from basaltic to picritic magmas that experienced little metasomatic overprint or loss of partial melt following eclogitization.

A positive Eu anomaly is a unique and unequivocal tracer of the low-pressure phase plagioclase, betraying that the protoliths of eclogites with this signature were originally low-pressure cumulates. These eclogites may be quartz-/coesite-bearing, but many are kyanite- and/or corundum-bearing with Ca-rich garnets and jadeite-rich clinopyroxenes, i.e., kyanite/corundum eclogites and grospydites. Such highly aluminous xenoliths have been rarely studied in detail because the jadeite-rich clinopyroxenes are highly reactive toward kimberlite magmas, leading to poor preservation in the xenolith record worldwide. Here, we describe kyanite- and corundum-bearing xenoliths from the Bellsbank diamond mine in South Africa that contain unusually fresh, primary, jadeite-rich clinopyroxene cores of sufficient size and quality to carry out a detailed study of their mineral major and trace element contents and isotope systematics. The aim of this paper was to identify the magmatic protoliths using major and trace elements and to constrain the evolutionary processes which led to their present-day mineralogy and chemistry. In addition, we place age constraints on the protoliths and make inferences about the nature of the parental ancient oceanic crust and its subsequent subduction.

Geological setting and sample description

The 118 ± 3-Ma-old Group II kimberlite fissures from Bellsbank (Smith et al. 1985) are situated approximately 100 km northwest of Kimberley, South Africa, roughly in the center of the West block of the Kaapvaal craton. The eclogite and garnet pyroxenite xenoliths found there range from garnet + clinopyroxene only to opx-, quartz-, kyanite-, and corundum-bearing varieties. Representative samples of each group have been studied previously mainly by Taylor and Neal (1989) and Neal et al. (1990) for their major and trace elements plus some Sm–Nd and oxygen isotope work. We collected a new suite of 2- to 5-cm sized samples of all varieties from the coarse concentrate dumps of the mine and report here on two samples that contain, besides garnet and clinopyroxene, kyanite (BE1 and BE13), and three samples with corundum (BE11, BBw, and BE6). We also include in the study an additional three samples (BBm, BBu, and BBs) which are assumed to be kyanite-/corundum (ky, cor)-bearing because the major and trace element compositions of their garnets and clinopyroxenes fall within the distinctive range of kyanite- and/or corundum-bearing samples. The ky/cor eclogites are coarse equant textured with light brown to orangy grt and light green cpx grains ranging between 3 and 5 mm in size. Blue kyanites in BE1 and BE13 are stubby and 2–3 mm long. Almost colorless to light pinkish corundum occurs as 1- to 2-mm ovals. The clinopyroxenes appear to have been dissolved along their rims and along cracks by reaction with the kimberlite magma, forming secondary cpx, phlogopite, K-feldspar, and carbonates. In this paper, we use the term "eclogite" alone when discussing these aluminous samples.

Analytical methods

Garnets, clinopyroxenes, and the Al phases were analyzed for major and trace elements and oxygen isotope ratios using electron microprobe, laser ablation ICP-MS, and laser fluorination, respectively, in Frankfurt. Sr isotope ratios of the clinopyroxenes were measured by solution MC-ICP-MS in Frankfurt, and duplicates of some samples were re-picked and analyzed by high-precision TIMS in Edmonton. Oxygen isotope compositions of garnets, clinopyroxenes, and kyanite were determined at Frankfurt and the University of Oregon using the methods described below.

Major element analysis

Major elements were measured by EPMA in the wavelength-dispersive mode (WDS) with a JEOL JXA 8900RL. Multiple grains of minerals from each sample were mounted in epoxy, polished, and analyzed in three to six spots on each grain to test for compositional homogeneity. The acceleration potential was 15 kV, the beam current 20 nA, and the spot size 3 μm. Counting times varied between 40 and 20 s on peak and background. Sodium was measured at the beginning of the measuring sequence for 20 s each on peak and one background. This and the

defocused beam were taken as a precaution to prevent the "loss" of Na during measurement from the pyroxenes.

Trace element analysis

The trace elements were analyzed by LA-ICP-MS using a New Wave Research LUV213TM ultraviolet Nd-YAG laser coupled with a Finnigan Element 2. The laser pulse frequency was 10 Hz with an energy pulse of 0.6–0.8 mJ (corresponding to an on-sample laser energy density of 3–5 J/cm^2 as measured with an external energy density meter). In order to minimize oxide formation, the UO^+/U^+ was tuned to less than 1 %. Spot sizes were 60–95 μm. NIST 612 glass was used as a calibration standard. USGS BIR-1 glass (abundances from Eggins et al. 1997) was the external and Ca from microprobe analysis of the minerals the internal standard. BIR-1 glass and one in-house garnet standard (PN2b; a megacryst from the young volcanics of the Jos Plateau in Nigeria) were measured several times within each sequence. Average abundance data obtained for BIR-1 and PN2b are presented in Table A1. The error for most elements obtained from 54 analyses on BIR-1 basalt glass is around 10 % over 2 years. The error for most elements is less than 10 % and rises to 15 % for elements with low abundances such as Ta and Th. The data reduction and abundances were processed online using the GLITTER software. Three to 10 analyses were carried out on random pieces of each crushed, fresh garnet, and clinopyroxene. They showed no differences outside the analytical errors, i.e., they are homogeneous within analytical error.

Sr isotope analysis

The Sr isotope ratios were analyzed in the clinopyroxene separates by MC-ICP-MS in Frankfurt and in four of them as duplicates in Edmonton by TIMS. The clinopyroxenes were coarsely crushed to separate larger pieces of primary cpx. These were recrushed and handpicked to separate any secondary pyroxene and alteration products. The separates were leached at room temperature in 6 M HCl for about half an hour and then ultrasonically cleaned with MQ H_2O twice before finally drying. After leaching, the grains were repicked to optical purity. Finally, 30–50 mg was used for solution chemistry in Frankfurt and only a few mg for solution chemistry in Edmonton. In Frankfurt, samples were dissolved in Teflon vials in a mixture of concentrated HF:HNO_3 (3:1). The Sr was purified in 1-ml Ln Spec resin columns (for details see Lazarov 2008). The accuracy of the Sr isotope ratio measurements was monitored by repeat measurements of the 200-ppb NIST SRM 987 standard. It gave an average value of $^{87}Sr/^{86}Sr = 0.71024 \pm 0.00003$ (2SD, $n = 6$). The chemistry blank is very low, only a few picograms, and is negligible.

The advantage for measuring the Sr isotope ratios by TIMS is that only 2–3 mg clean clinopyroxene separates are needed (corresponding to a few ng Sr) so that the danger of analyzing contaminated mineral separates is minimized. Samples were dissolved in 2 ml of concentrated HF + HNO_3 and purified using custom-built Teflon columns containing 0.05 ml of Eichrom Sr-Spec resin (Sarkar et al. 2015 and references therein). Purified Sr was loaded onto single rhenium filaments using a tantalum gel loading technique (Creaser et al. 2004). Sr isotopic compositions were determined using Faraday cup detectors in a static multi-collector mode. Accuracy and instrument stability were monitored by repeated measurements of the NIST SRM 987 standard, which gave an average value of $^{87}Sr/^{86}Sr = 0.71026 \pm 0.00006$ (2SD, $n = 3$) during the measuring period. The chemistry blank was 2–3 pg.

Oxygen isotope analysis

The oxygen isotope ratios of the garnets and primary clinopyroxenes from three samples were determined by the CO_2-laser fluorination technique with a strongly oxidizing BrF_5 reagent connected to a gas source mass spectrometer at Frankfurt University (laboratory Dr. Jens Fiebig). We also analyzed secondary cpx and kyanite in one sample. Five additional samples were analyzed at the University of Oregon—Bindeman Laboratory. Optically clean pieces of the minerals weighing 1.5–2.0 mg were handpicked for the analysis. In Frankfurt, quartz Lausanne-1 ($\delta^{18}O = +18.15$ ‰; Allaz et al. 2005) and garnet UWG-2 ($\delta^{18}O = +5.89$ ‰; Valley et al. 1995) were used as reference standards. The reproducibility (2 s) on the garnet standard was ±0.1 ‰ and on the quartz standard ±0.24 ‰. A larger variability in the quartz standard was already observed in previous work (e.g., Kusakabe et al. 2004). The precision of standards at the University of Oregon is better than 0.1 ‰ (1 s; Bindeman et al. 2012).

Results

Major elements and geothermobarometry

The major element compositions of the garnets and clinopyroxenes are given in Table 1a, b and shown in Fig. 1a, b and in the electronic appendix in Fig. A1 a,b. Garnets and clinopyroxenes are homogeneous within the analytical error. Garnets plot in the eclogite classification diagram of Coleman et al. (1965) within field B, with grossular and pyrope contents ranging from 31–45 to 33–53 mol%, respectively (Fig. A1a). Garnets and clinopyroxenes have very low Cr and Ti contents. The clinopyroxenes are jadeite-rich with Na_2O ranging between 6 and

Table 1 Major element compositions of (a) garnets and the structural formula (12 O), (b) clinopyroxene and the structural formula (6 O)

Sample	BE1	BE6	BE11	BE13	BBm	BBs	BBu	BBw
(a)								
Major element compositions of garnet (wt%)								
SiO_2	41.20	41.81	40.65	40.24	41.06	41.90	40.91	41.12
Na_2O	0.08	0.06	0.07	0.05	0.04	0.05	0.05	0.04
CaO	17.29	12.14	17.66	14.42	12.81	15.09	11.96	14.57
MnO	0.17	0.18	0.22	0.19	0.21	0.18	0.18	0.13
MgO	9.10	11.98	8.62	10.07	12.75	8.93	12.57	12.58
Cr_2O_3	0.06	0.25	0.04	b.d.l.	0.06	0.01	0.04	b.d.l.
FeO^{total}	10.74	12.63	11.18	12.49	10.62	11.94	11.70	8.90
Al_2O_3	22.78	22.94	22.02	22.86	23.09	23.19	23.17	23.21
TiO_2	0.16	0.15	0.15	0.15	0.09	0.10	0.15	0.08
NiO	0.04	0.02	0.02	0.02	0.02	0.02	0.02	0.03
Total	101.63	102.06	100.63	100.52	100.75	101.43	100.74	100.70
Mg#	60	63	58	59	68	49	66	72
Structural formula (12 O)								
Si	3.009	3.012	3.013	2.975	2.987	3.006	2.982	2.983
Na	0.011	0.008	0.010	0.007	0.006	0.006	0.007	0.005
Ca	1.353	0.939	1.403	1.143	0.998	1.614	0.934	1.133
Mn	0.011	0.011	0.014	0.012	0.013	0.011	0.011	0.008
Mg	0.990	1.289	0.952	1.110	1.382	0.687	1.366	1.360
Cr	0.003	0.014	0.002	0.000	0.003	0.000	0.002	0.000
Fe	0.656	0.762	0.693	0.772	0.646	0.716	0.713	0.540
Al	1.961	1.953	1.923	1.992	1.979	1.961	1.991	1.984
Ti	0.009	0.008	0.008	0.008	0.005	0.006	0.008	0.005
Ni	0.002	0.001	0.001	0.001	0.001	0.001	0.001	0.002
Total	8.007	7.999	8.019	8.022	8.020	8.009	8.016	8.021

Sample	BE1	BE6	BE11	BE13	BBm	BBs	BBu	BBw
(b)								
Major elements compositions of clinopyroxene (wt%)								
SiO_2	56.56	56.86	55.93	55.26	55.56	56.67	55.41	55.55
Na_2O	9.01	8.24	9.17	6.36	7.71	6.55	6.59	8.44
CaO	10.18	11.53	9.88	13.71	12.21	9.55	13.13	11.18
MnO	b.d.l.	0.01	0.01	0.02	0.02	0.02	0.02	0.01
MgO	5.98	7.22	5.85	8.15	8.03	13.93	7.67	6.98
Cr_2O_3	0.06	0.34	0.04	0.02	0.08	0.02	0.04	0.01
FeO^{total}	1.42	1.70	1.57	1.88	1.41	2.06	1.28	0.91
Al_2O_3	16.93	14.53	17.16	13.91	14.26	11.48	15.37	16.26
TiO_2	0.19	0.21	0.14	0.20	0.14	0.20	0.21	0.09
NiO	0.17	0.21	0.09	0.08	0.16	0.18	0.10	0.18
Total	100.51	100.85	99.84	99.61	99.58	100.68	99.84	99.60
Mg#	88	88	87	89	91	90	91	93
Structural formula (6 O)								
Si	1.958	1.974	1.950	1.949	1.955	1.984	1.939	1.944
Na	0.605	0.554	0.620	0.435	0.526	0.444	0.447	0.572
Ca	0.378	0.429	0.369	0.518	0.460	0.498	0.492	0.419
Mn	0.000	0.000	0.000	0.001	0.001	0.001	0.000	0.000
Mg	0.309	0.373	0.304	0.428	0.421	0.522	0.400	0.364
Cr	0.002	0.009	0.001	0.000	0.002	0.001	0.001	0.000
Fe	0.041	0.049	0.046	0.056	0.042	0.060	0.037	0.027
Al	0.691	0.595	0.705	0.578	0.592	0.474	0.634	0.671
Ti	0.005	0.006	0.004	0.005	0.004	0.005	0.006	0.002
Ni	0.005	0.006	0.002	0.002	0.004	0.005	0.003	0.005
Total	3.993	3.995	4.002	3.974	4.007	3.995	3.961	4.004

b.d.l. below detection limit

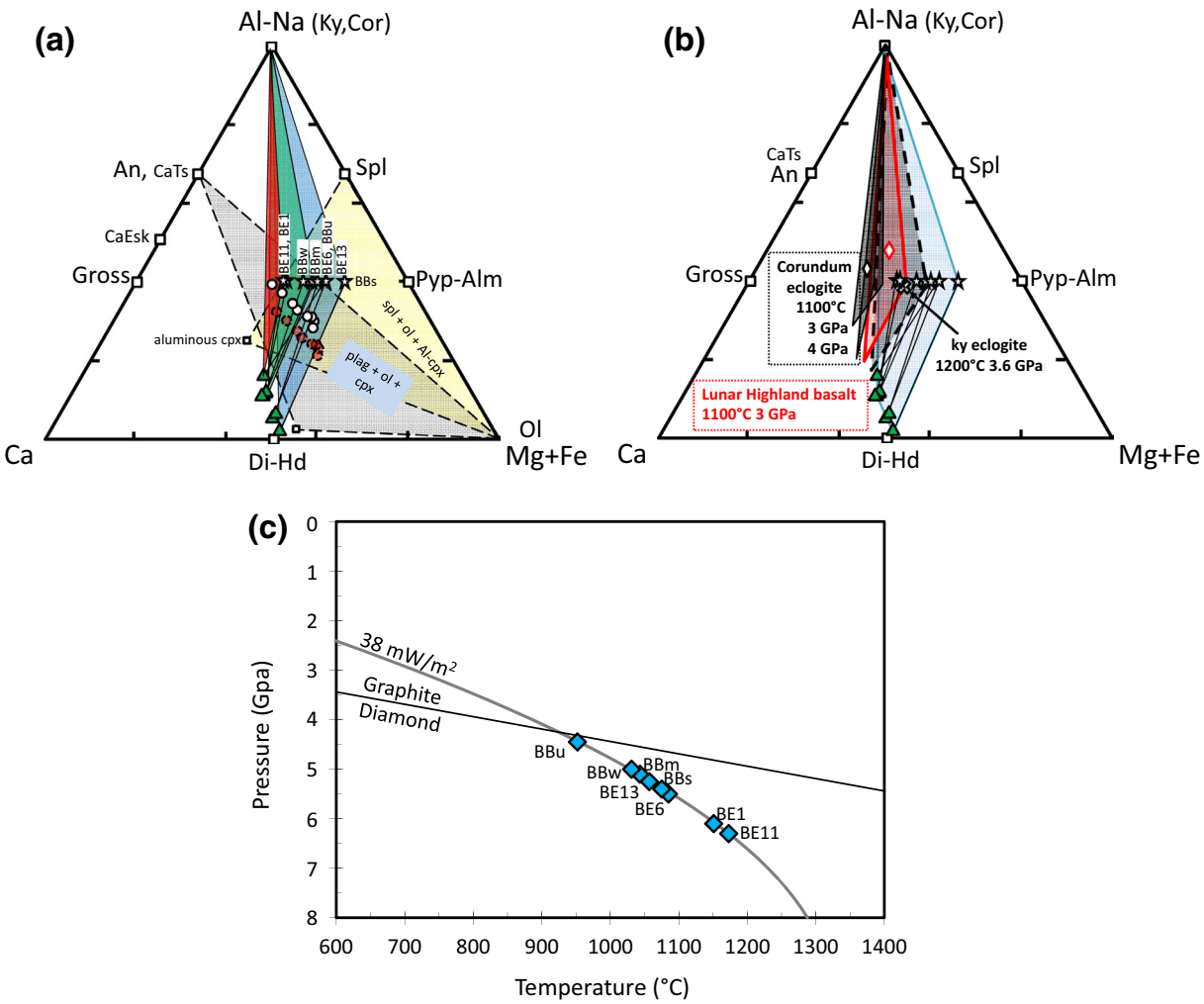

Fig. 1 **a** Composition of coexisting garnets and clinopyroxenes in a phase diagram of (Al–Na)–Ca–(Mg + Fe^{total}) in atomic proportions projected from Si. Kyanite and corundum plot on the (Al–Na) corner, olivine, and opx on (Mg + Fe) and spinel and pyrope-almandine in between. Anorthite (and all plagioclase solid solutions) and the Ca-Tschermaks component plot 2/3 along the Ca–(Al–Na) join and the Ca-Eskola component in the middle. The clinopyroxenes of our samples extend in composition along the join (Di-Hd)–Ca-Tschermaks, and the garnets vary between 31 and 45 mol% grossular. The tie lines between grt and cpx differ in slope which corresponds to varying temperatures. Also shown are compatibility triangles for potential lower pressure protoliths. These could be at the lowermost pressures cumulates of mainly olivine and plagioclase or, at somewhat elevated pressures, cumulates of olivine, spinel, and aluminous clinopyroxenes. Calculated ($grt_{60}cpx_{40}$) bulk rock compositions of the eclogites are shown by *red circles*. These compositions were shifted toward the (Al–Na) apex by an arbitrary 2 % Al_2O_3 to account for the unknown modal amounts of kyanite and corundum (*white circles*). **b** Compositions of coexisting grt and cpx from experiments at 1100 and 1200 °C and 3–4 GPa on a corundum eclogite (*black diamond*; Morishita et al. 2004), a lunar highland basalt (*red diamond*; Råheim and Green 1974) and a kyanite eclogite (*black cross*; Green 1967). The Al contents of Bellsbank eclogite clinopyroxenes are lower than those from experiments, i.e., they are derived from higher pressures. **c** Pressures and temperatures of last equilibration of the Bellsbank eclogites. Temperatures were calculated with the Fe–Mg exchange thermometer between grt and cpx in the version of Krogh (1988) and projected onto a conductive geothermal gradient of 38 mW/m^2 (Chapman and Pollack 1977)

9.5 wt% (Fig. A1b), with high Al_2O_3 contents between 11 and 17 wt%, FeO less than 2 wt%, MgO between 6 and 10 wt%, and CaO between 9.5 and 14 wt%. Kyanite and corundum have small amounts of Cr and Mn as their most significant impurities. The sum of cations is 3.974 in clinopyroxenes from sample BE13 and 3.961 in cpx's from BBu. The Al in the structural formula is higher than the sum of tetrahedrally coordinated Al (=2-Si) and of Na so that a Ca-Eskola component is needed for charge balance. The Tschermaks, jadeite, and Ca-Eskola components in the structural formula based on six oxygens are 0.102, 0.435, and 0.041 for BE13 and 0.122, 0.447, and 0.246 for BBu.

The Ca-Eskola component indicates a high SiO_2 activity in the rocks and requires at least modal kyanite and possibly a SiO_2 phase in the eclogites (the Eskola components plot along a dividing line between kyanite + SiO_2 and kyanite alone in Fig. 11a of Knapp et al. 2013). Importantly, these samples are those with the largest positive Eu and Sr anomalies and the least depleted LREE (see section on partial melting below).

Figure 1a shows the compositions of coexisting garnets and clinopyroxenes in a triangular diagram of (Al–Na)–Ca–(Mg + Fe^{total}) in atomic proportions projected from Si. Shortcomings of such a diagram are that differences in the Mg values of the bulk rocks and constituent minerals cannot be shown, that corundum and kyanite plot together onto the (Al–Na) apex, that all plagioclase compositions plot as anorthite, and that the Al content of the clinopyroxenes is presented only in terms of the Tschermaks and Ca-Eskola component, whereas jadeite cannot be shown. Nonetheless, the plot is one of the few that allows to display most aspects of the compositional relationships between all the phases in the rocks at once and simultaneously those of potential precursor rocks. The garnets from the Bellsbank eclogites plot to the right of the line between (Al–Na) and (Di–Hd) with grossular varying between 31 and 45 mol% and the omphacites plotting near the Ca–(Mg + Fe) base of the triangle. The latter extend from (Di–Hd) toward the Ca-Tschermaks component. The coexisting garnets and clinopyroxenes are connected by tie lines, and compatibility triangles are drawn for three samples which cover the pressure, temperature range of the eclogites. For comparison, schematic compatibility diagrams are shown for two equivalent lower pressure assemblages of potential protoliths of the eclogites, i.e., olivine + plagioclase + Al-bearing clinopyroxenes at the lowest pressures and olivine + Al-rich clinopyroxene + spinel at somewhat elevated pressures (the distinction can be made by the presence or absence of a positive Eu anomaly; see discussion below).

Figure 1b shows the comparison with compatibility triangles for a few selected *P*, *T* conditions of high-pressure experiments up to 4 GPa by Morishita et al. (2004), Råheim and Green (1974), and Green (1967) on a corundum eclogite, a lunar highland basalt (that crystallizes to a kyanite eclogite in experiments at high pressures), and a kyanite eclogite, respectively. It can be seen that the clinopyroxenes from the high-pressure experiments are Al-richer (=have higher Ca-Tschermaks contents) than those from the Bellsbank eclogites.

Bulk rock chemical analyses have only limited significance because of the small sample sizes and the interaction with the kimberlite magma. We therefore calculated bulk rock compositions from primary mineral compositions by using 60 % garnet and 40 % cpx (visual estimates). The results are given in the appendix in Table A2, shown as red and white dots in Fig. 1a and as summarized fields in oxide variation diagrams in Figs. 2a, b and A2 a-c. The red dots and fields correspond directly to the calculated compositions, and the white dots and fields are shifted arbitrarily corresponding to about 2 % more Al_2O_3 to account for modal kyanite and/or corundum. The figures also show the bulk rock compositions of troctolites from the Pito Deep in the Pacific ocean (Perk et al. 2007) and of troctolites and olivine gabbros from the Kane Fracture Zone on the Mid-Atlantic rise (MARK; Casey 1997). Also given in these figures is the range of the olivine and plagioclase compositions (connected by tie lines; taken from Perk et al. 2007; Coogan 1998; Coogan et al. 2000) in these cumulates and the tie lines for coexisting garnets and omphacites of the Bellsbank eclogites. The comparison with MARK and Pito Deep shows that the eclogites overlap in SiO_2 with the troctolites from MARK and the troctolites from the Pito Deep from more evolved melts (Fig. 2a), but that they are Na_2O (Fig. 2b) and FeO (Fig. A2b) richer than both including the olivine gabbros from MARK.

The Fe-rich nature is seen in Fig. 2c, a diagram of Ni against Mg# (100 × Mg/(Mg + Fe). The Bellsbank eclogites have much lower Mg# and simultaneously much higher Ni (and Co) contents (relative to Mg#) than the oceanic samples. The Bellsbank data points labelled in pink are from the samples with the strongest LREE depletion (see below).

Although the phase equilibria experiments cited above were carried out at pressures less than those corresponding to relevant temperatures along a cratonic geothermal gradient, it is quite apparent from the comparison of the experimental results and the natural rocks that the eclogite xenoliths stem from much higher pressures. The *P*, *T* conditions of last equilibration of the eclogites can be estimated by projecting the temperatures of a Fe–Mg grt-cpx exchange thermometer onto a conductive geothermal gradient (Chapman and Pollack 1977), and we assume 38 mW/m^2 for Bellsbank. The Krogh (1988) Fe–Mg exchange thermometer was applied, instead of more recent variations in this thermometer, because it is confirmed by the experiments of Purwin et al. (2012) who evaluated the influence of Fe^{3+} on the grt-cpx thermometer, and found it to be negligible. The dominant uncertainties in this kind of geothermobarometry are a combination of the slope of the chosen geothermal gradient within the temperature range under consideration (here around 120 °C/GPa), the pressure dependency of the thermometer (around 40 °C/GPa) and the experimental uncertainty of the thermometer (around ±30 °C). The first two uncertainties do not change the relative positions of the samples in P and T, while the latter error determines whether the *P*, *T* conditions are distinguishable between the samples. The steepening of the *P*, *T* slope of conductive geothermal gradients at higher temperatures, toward the

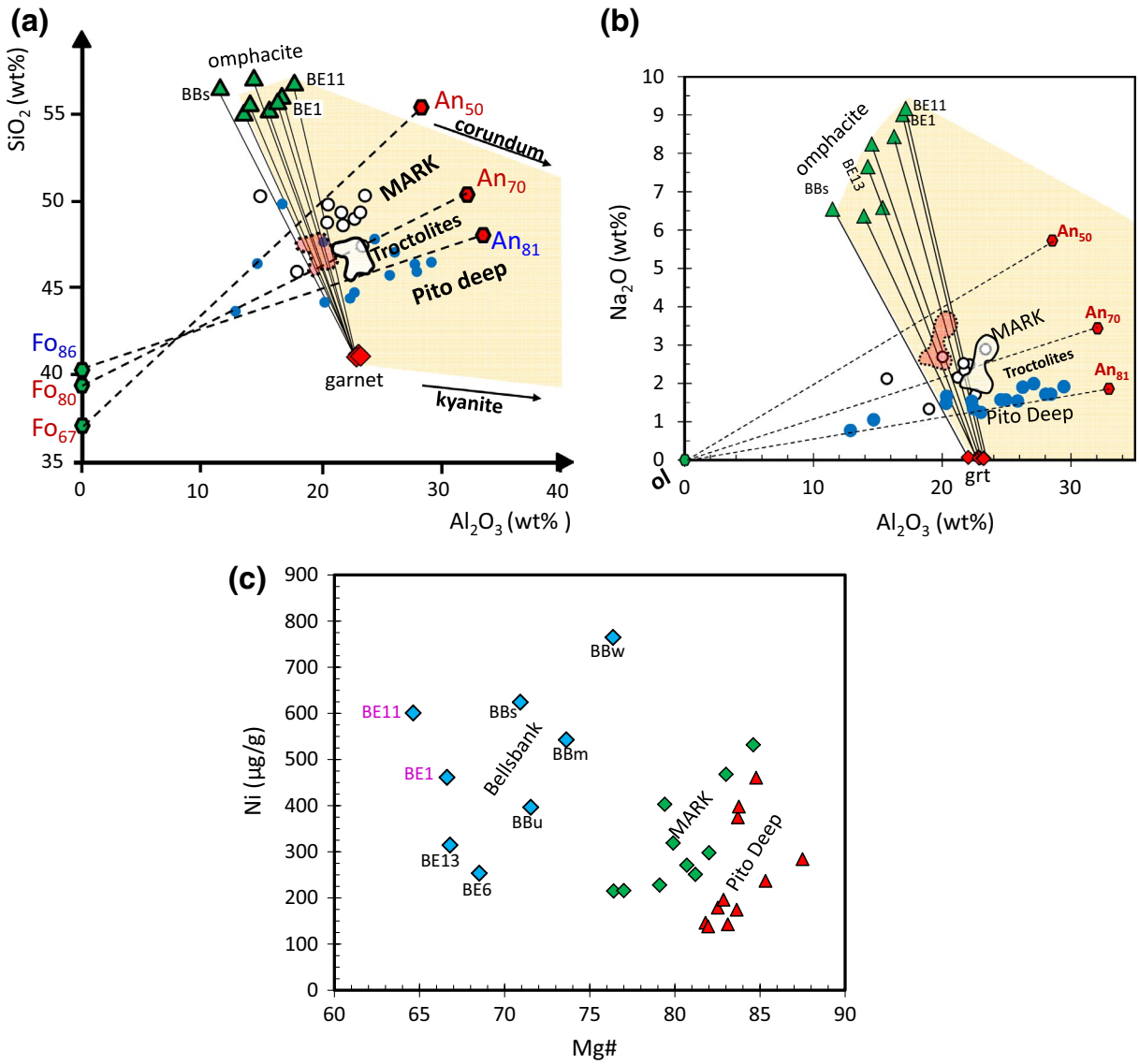

Fig. 2 **a** SiO_2 versus Al_2O_3 showing the compositions of coexisting olivines (Fo_{86}) and plagioclases (An_{81}) of troctolitic cumulates from the Pito Deep and their bulk rock compositions (*blue dots*) plus the more evolved olivine and plagioclase compositions from cumulate rocks of the MARK area (bulk rocks = *black circles*). The *pink field* comprises the range of calculated bulk rock compositions, and the *white field* is the arbitrary shift to higher Al_2O_3 to account for the unknown modal amounts of kyanite and corundum. **b** The variation in Na_2O with Al_2O_3 for the Bellsbank clinopyroxenes and the MARK and Pito Deep cumulates. **c** Ni contents in the calculated bulk rocks of the Bellsbank eclogites plotted against Mg# in comparison with the cumulates from MARK and the Pito Deep

transition to a convective geothermal gradient, combined with the positive P, T dependence of the slope of the K_D of the Fe–Mg exchange thermometer, results in pressures that are overestimated at higher temperatures and, eventually, K_D and geothermal gradient do not intersect anymore. This problem is aggravated by the choice of a colder geothermal gradient and is clearly apparent in the work of Gréau et al. (2011) who choose a very cold geothermal gradient (35 mW/m^2) for Roberts Victor (another eclogite locality on the Kaapvaal craton) that significantly steepens between 1000 and 1100 °C. To circumvent this problem, they introduced an unwarranted kinked geotherm which then creates the misleading impression of an eclogite layer that is concentrated along the lithosphere–astenosphere boundary at Roberts Victor. We choose 38 mW/m^2 to be consistent with our earlier work (Shu et al. 2014). For this geotherm, sample BBu gives 950 °C at 4.5 GPa, five samples (BBw, BBm, BE13, BBs, and BE6) originate (within the probable error of the P, T estimation procedure) from similar depths corresponding to about 5.3 GPa and 1050 °C, and two samples (BE1 and BE11) from about 1160 °C and 6.3 GPa (Fig. 1c). The choice of a hotter geothermal

Table 2 Averaged trace element compositions of garnets (μg/g)

Sample	BE1 grt	RSD (%)	*N*	BE6 grt	RSD (%)	*N*	BE11 grt	RSD (%)	*N*	BBu grt	RSD (%)	*N*
Li	0.44	7	7	0.39	9	10	0.56	5	7	0.52	15	9
Sc	21	3	7	17	3	10	46	5	7	23	5	9
Ti	1265	2	7	1130	5	10	1054	4	7	1084	3	9
V	274	4	7	119	4	10	257	2	7	57	3	9
Cr	315	4	7	1513	3	10	293	4	7	259	2	9
Mn	1468	4	7	1351	1	10	1734	3	7	1304	3	9
Co	64	4	7	88	3	10	63	4	7	97	3	9
Ni	114	2	7	154	2	10	63	5	7	108	3	9
Ga	9.2	6	7	8.0	2	10	10.3	40	7	7.6	5	9
Rb	0.031	38	7	0.037	50	9	n.d.	44	2	0.075	32	4
Sr	0.17	28	7	0.09	15	9	0.12	71	6	2.89	8	9
Y	8.0	7	7	4.9	3	9	15.7	4	7	5.5	5	9
Zr	2.3	22	7	4.9	5	9	2.4	12	7	2.1	20	9
Nb	0.003	20	6	0.008	76	10	0.088	31	4	0.414	35	6
Ba	0.008	16	4	n.d.			0.929	93	5	0.659	36	7
La	0.026	86	7	0.019	19	10	0.124	44	7	0.049	50	9
Ce	0.344	7	7	0.166	14	10	0.378	17	7	0.258	14	9
Pr	0.051	79	7	0.036	29	10	0.032	23	7	0.076	8	9
Nd	0.605	6	7	0.228	27	10	0.128	13	7	0.567	7	9
Sm	0.249	15	7	0.283	2	10	0.373	5	7	0.318	9	9
Eu	0.263	5	7	0.337	2	10	0.306	4	7	0.297	6	9
Gd	0.529	8	7	0.516	3	10	1.411	4	7	0.568	6	9
Tb	0.141	11	7	0.125	3	10	0.317	7	7	0.118	6	9
Dy	1.357	8	7	0.946	3	10	2.629	6	7	0.949	6	9
Ho	0.299	7	7	0.192	3	10	0.615	5	7	0.221	4	9
Er	0.923	7	7	0.530	5	10	1.895	2	7	0.686	5	9
Tm	0.142	9	7	0.085	5	10	0.287	2	7	0.101	9	9
Yb	1.106	7	7	0.619	4	10	2.097	4	7	0.728	5	9
Lu	0.135	9	7	0.079	5	10	0.330	5	7	0.109	5	9
Hf	0.056	11	7	0.093	9	10	0.099	21	7	0.082	9	9
Ta	0.0044	40	5	0.0013	24	3	0.0254	114	7	0.9822	168	9
Pb	0.0036	53	7	0.0053	99	10	0.1403	70	7	0.1561	55	9
Th	0.0257	28	7	0.0327	109	10	0.1246	27	7	0.0048	205	8
U	0.0387	13	7	0.0257	90	10	0.0770	38	7	0.0085	84	9
Sample	BBw grt	RSD (%)	*N*	BBm grt	RSD (%)	*N*	BBs grt	RSD (%)	*N*	BE13 grt	RSD (%)	*N*
Li	0.32	5	8	0.37	7	6	0.55	5	7	0.70	4	5
Sc	10	2	8	31	2	6	10	2	7	13	4	5
Ti	547	3	8	668	4	6	704	4	7	1057	2	5
V	20	2	8	56	3	6	15	2	7	23	2	5
Cr	74	3	8	418	2	6	92	2	7	48	2	5
Mn	1074	1	8	1632	2	6	1405	1	7	1462	2	5
Co	82	2	8	81	1	6	104	1	7	91	2	5
Ni	203	4	8	117	4	6	122	2	7	69	4	5
Ga	6.6	4	8	6.4	2	6	6.5	2	7	6.3	3	5
Rb	n.d.			n.d.			n.d.			n.d.		
Sr	0.16	21	8	0.14	24	6	0.18	5	7	2.86	5	5
Y	4.2	3	8	7.6	3	6	3.9	4	7	5.9	7	5
Zr	5.0	9	8	2.6	8	6	7.8	6	7	7.2	4	5

Table 2 continued

Sample	BBw grt	RSD (%)	*N*	BBm grt	RSD (%)	*N*	BBs grt	RSD (%)	*N*	BE13 grt	RSD (%)	*N*
Nb	0.600	88	8	0.501	78	6	0.320	116	7	0.551	107	5
Ba	0.529	61	8	1.269	17	3	0.538	69	7	0.276	73	4
La	0.074	62	8	0.046	69	6	0.025	37	7	0.057	30	5
Ce	0.241	56	8	0.147	17	6	0.132	14	7	0.515	10	5
Pr	0.031	16	8	0.026	11	6	0.036	16	7	0.140	3	5
Nd	0.296	11	8	0.232	6	6	0.308	8	7	1.189	2	5
Sm	0.263	6	8	0.202	4	6	0.287	5	7	0.551	7	5
Eu	0.325	4	8	0.254	2	6	0.331	5	7	0.599	6	5
Gd	0.453	4	8	0.589	4	6	0.552	7	7	0.778	7	5
Tb	0.090	3	8	0.146	2	6	0.101	5	7	0.139	12	5
Dy	0.691	3	8	1.262	4	6	0.696	6	7	1.034	8	5
Ho	0.157	3	8	0.289	4	6	0.147	7	7	0.214	11	5
Er	0.489	5	8	0.902	3	6	0.419	6	7	0.641	8	5
Tm	0.075	4	8	0.140	6	6	0.063	6	7	0.092	6	5
Yb	0.549	3	8	1.046	5	6	0.434	5	7	0.674	7	5
Lu	0.082	3	8	0.157	6	6	0.067	3	7	0.099	9	5
Hf	0.105	14	8	0.069	13	6	0.127	14	7	0.136	5	5
Ta	0.5625	101	8	0.3807	81	6	0.2157	119	6	0.4093	49	5
Pb	0.2846	77	8	0.2009	70	6	0.1952	41	7	0.0389	66	5
Th	0.0504	40	8	0.0270	14	6	0.0119	15	7	0.0020	84	5
U	0.0539	91	8	0.0309	64	6	0.0179	40	7	0.0137	141	5

gradient (e.g., 40 mW/m^2 with a flatter slope) would shift the samples to somewhat lower *P*, *T* conditions and narrow the *P*, *T* interval between them.

Trace elements

Averaged trace element contents of the garnets and clinopyroxenes are given in Tables 2 and 3 and presented as PM (primitive mantle)-normalized (McDonough and Sun, 1995) trace element patterns (U, Ba, Sr + REE) in Fig. 3a. Both garnets and clinopyroxenes have very pronounced positive Eu anomalies, except for the corundum eclogite BE11. Garnet middle to heavy REE patterns are flat to slightly positively inclined, with abundances of one to two times that of the PM (except for BE11 where Lu is 5 times PM). The light REE are depleted to various extents, but La and in some cases Ce and Pr are elevated in several samples. The cpx trace element patterns have negative slopes with low HREE between 0.01 and 0.02 times PM and positive Eu anomalies in all samples but BE11. The normalized patterns are complementary to those of the garnets and correspond to equilibrium partitioning. Equilibrium is indicated for the REE by the comparison of the grt/cpx partition coefficients of the eclogites with experimentally determined K_D's, e.g., those of Green et al. (2000) at 3 and 4 GPa and 1100 to 1200 °C (Fig. A3). The partitioning for the natural rocks runs parallel to the experimental K_Ds but at higher values, most likely because of the higher Na contents of the clinopyroxenes. The Sr contents are very low in six garnets and their coexisting clinopyroxenes but significantly elevated in cpx from two samples (BBu and BE13; 221 and 232 µg/g). There are no Ti, Zr, and Hf anomalies, and Nb and Ta are near or below the detection limits.

Figure 3b shows the calculated, PM-normalized bulk rock trace element compositions for assumed modal amounts of grt and cpx of 60 and 40 % (visual estimation of the modal proportions in the small samples; calculated major and trace element contents are given in the electronic appendix in Table A2). Jacob and Foley (1999) showed that for grt:cpx ratios between 50:50 and 70:30, the calculated abundance patterns do not change significantly, and important geochemical features remain very similar, which allows us to make meaningful deductions from them. In all our trace element diagrams, we have placed Sr before La in order to clearly visualize the LREE patterns. All samples, except BE11, have MREE and HREE abundances close to that of the primitive mantle. The two samples with highest Sr contents (red patterns in Fig. 3b) have flat middle to heavy REE patterns with abundances lower than that of PM and with slightly depleted LREE. The sample with the third highest Sr content (green pattern) has flat middle to heavy REE but negatively inclined LREE from La to Nd. Four samples (black patterns) have positively inclined HREE (with abundances higher and lower than PM), while

Table 3 Averaged trace element compositions of clinopyroxenes (μg/g)

Sample	BE1 cpx	RSD (%)	*N*	BE6 cpx	RSD (%)	*N*	BE11 cpx	RSD (%)	*N*	BBu cpx	RSD (%)	*N*
Li	11.39	3	6	10.44	4	10	15.08	3	8	11.09	3	10
Sc	10	11	6	9	4	10	6	4	8	5	3	10
Ti	1505	4	6	1632	5	10	1051	2	8	1522	4	10
V	705	4	6	456	4	10	679	3	8	151	8	10
Cr	291	2	6	1772	4	10	314	2	8	316	2	10
Mn	59	4	6	98	58	10	72	2	8	95	6	10
Co	15	4	6	22	5	10	16	1	8	29	4	10
Ni	982	4	6	1271	4	10	540	2	8	829	6	10
Ga	26.5	3	6	25.7	2	10	23.9	4	8	20.2	3	10
Rb	0.221	40	6	0.030	57	6	0.035	54	4	0.113	98	10
Sr	9.89	4	6	12.29	4	10	4.37	3	8	232.87	7	10
Y	0.1	15	6	0.1	13	10	0.1	9	8	0.1	11	10
Zr	0.4	47	6	2.0	8	10	0.4	38	8	1.1	19	10
Nb	n.d.			0.019	69	10	0.038	44	8	0.753	172	10
Ba	n.d.			0.037	93	9	0.243	95	5	2.813	32	10
La	0.283	30	6	0.333	2	10	0.361	5	8	0.449	9	10
Ce	0.568	33	6	0.689	8	10	0.436	4	8	1.075	6	10
Pr	0.066	27	6	0.079	6	10	0.016	13	8	0.131	6	10
Nd	0.221	25	6	0.270	3	10	0.034	21	8	0.509	6	10
Sm	0.030	17	6	0.061	9	10	0.030	34	8	0.080	9	10
Eu	0.019	29	6	0.036	6	10	0.014	19	7	0.048	5	10
Gd	0.040	18	5	0.047	13	10	0.043	26	7	0.068	14	10
Tb	0.006	43	6	0.006	22	10	0.006	33	8	0.007	13	10
Dy	0.022	33	6	0.026	13	10	0.033	29	8	0.033	15	10
Ho	0.004	21	5	0.003	21	10	0.009	91	8	0.005	25	10
Er	0.017	52	5	0.009	33	7	0.010	32	8	0.010	18	10
Tm	0.005	29	5	0.001	37	7	0.002	73	7	0.001	48	10
Yb	0.005	42	5	0.005	38	8	0.007	13	6	0.007	30	8
Lu	0.002	45	5	0.001	54	8	0.001	84	5	0.001	15	9
Hf	0.059	28	6	0.179	12	10	0.059	12	8	0.103	15	10
Ta	n.d.			0.0076	110	6	0.0093	98	6	0.8947	347	6
Pb	0.0151	50	6	0.0275	67	10	0.2412	48	8	0.1555	61	10
Th	0.0085	30	6	0.0362	12	10	0.0611	18	8	0.0025	80	10
U	0.0063	62	6	0.0084	114	10	0.0121	117	8	0.0223	101	10
Sample	BBw cpx	RSD (%)	*N*	BBm cpx	RSD (%)	*N*	BBs cpx	RSD (%)	*N*	BE13 cpx	RSD (%)	*N*
Li	13.00	6	5	12.11	2	6	10.99	3	8	14.31	2	5
Sc	2	2	5	4	1	6	3	2	8	3	3	5
Ti	649	2	5	988	3	6	1452	3	8	1405	2	5
V	76	1	5	205	2	6	78	2	8	57	5	5
Cr	100	2	5	527	1	6	143	1	8	55	1	5
Mn	50	2	5	78	2	6	92	6	8	97	6	5
Co	19	1	5	21	1	6	29	3	8	35	1	5
Ni	1607	2	5	1181	1	6	1378	2	8	683	1	5
Ga	20.1	1	5	18.2	1	6	18.0	1	8	15.7	4	5
Rb	n.d.			n.d.			0.034	53	3	0.083	85	4
Sr	10.53	2	5	14.95	2	6	72.56	1	8	221.46	4	5
Y	0.0	9	5	0.1	17	6	0.1	5	8	0.1	8	5
Zr	0.9	14	5	0.9	23	6	5.7	5	8	5.0	7	5

Table 3 continued

Sample	BBw cpx	RSD (%)	*N*	BBm cpx	RSD (%)	*N*	BBs cpx	RSD (%)	*N*	BE13 cpx	RSD (%)	*N*
Nb	0.461	122	5	0.306	28	6	0.496	82	7	1.246	85	5
Ba	0.338	58	4	0.372	119	4	0.581	109	8	2.518	68	5
La	0.391	5	5	0.393	3	6	0.916	6	7	0.614	6	5
Ce	0.437	9	5	0.606	5	6	2.129	4	7	1.621	5	5
Pr	0.029	10	5	0.044	3	6	0.212	5	7	0.194	2	5
Nd	0.120	9	5	0.164	7	6	0.808	3	7	0.750	5	5
Sm	0.026	14	5	0.034	9	6	0.162	6	7	0.098	6	5
Eu	0.019	11	5	0.023	5	6	0.090	3	7	0.061	3	5
Gd	0.020	19	5	0.039	13	6	0.098	10	7	0.107	73	5
Tb	0.003	31	5	0.004	11	6	0.008	12	7	0.006	20	5
Dy	0.011	11	5	0.020	15	6	0.031	12	7	0.024	20	5
Ho	0.004		1	0.003	18	5	0.003	29	7	0.004	19	5
Er	0.004	50	4	0.007	20	4	0.008	17	5	0.007	10	5
Tm	0.001	44	4	0.001	31	5	0.001	34	6	0.001	29	5
Yb	0.003		1	0.005	21	3	0.004	29	6	0.007	17	5
Lu	0.001	54	3	0.001	16	4	0.001	24	5	0.002	57	5
Hf	0.069	10	5	0.080	9	6	0.352	4	7	0.222	12	5
Ta	0.5528	102	5	1.0597	124	6	0.4265	48	7	3.7509	79	3
Pb	0.0628	20	5	0.0692	65	6	0.7425	29	7	0.1345	30	5
Th	0.0471	8	5	0.0555	4	6	0.0827	4	7	0.0023	59	5
U	0.0044	39	5	0.0150	107	6	0.0187	47	7	0.0161	77	5

the middle to light REE decline steeply toward the LREE beginning at Dy. They have the lowest Sr contents, but a positive Sr anomaly still exists if Sr is placed between Pr and Nd as is commonly done. The REE pattern of BE11 is similarly shaped to the black patterns at higher middle to heavy REE abundances, with more depleted LREE. The PM-normalized trace elements of the calculated bulk rocks are compared in Fig. 3c with troctolites and olivine gabbros from the Kane fracture zone on the Mid-Atlantic ridge (MARK; Casey 1997) and in Fig. 3d with troctolites from the Pito Deep in the Pacific Ocean (Perk et al. 2007).

The vanadium contents of six eclogites are well correlated with their Cr contents, with a slope (0.14) more than three times steeper than that defined by Pito Deep troctolites (0.042; Fig. 3e). We will use this clearly resolved difference in slope to estimate the offset in the oxygen fugacity of the crystallizing parent magmas (see below). The two eclogites plotting off the correlation line are those with the strongest LREE depletion (Fig. 3b) but also the lowest Mg# (Fig. 2c).

Oxygen isotope ratios

The $\delta^{18}O$ values of the garnets and primary clinopyroxenes, one kyanite, and one secondary cpx are given in Table 4 and shown in Fig. 4. The $\delta^{18}O$ values of the garnets fall within the same range as has been reported for the garnets of eclogites and garnet pyroxenites from Bellsbank previously (Neal et al. 1990). Four garnets vary around a $\delta^{18}O$ value of 4.5 ‰ and their coexisting cpx's around 4.9 ‰. The garnets are between 0.2 and 0.5 ‰ lower than the clinopyroxenes. The other four garnets lie between 2.5 and 3.8 ‰, and their coexisting cpxs are higher by about 0.5 ‰. The cpx from BE1 sample shows a much higher deviation of $\delta^{18}O$ from its garnet of 1.1 ‰. This is the same difference in the altered cpx in BBu to its garnet, while the difference in the unaltered cpx to garnet is similar to that in other samples (around 0.5 ‰). The extreme difference between cpx and grt BE1 may be partly due to impurities in cpx. The only measured kyanite from BE13 has an oxygen isotopic composition that falls between grt and cpx.

Strontium isotope ratios

The $^{87}Sr/^{86}Sr$ isotope ratios in handpicked separates of the primary clinopyroxenes range from extremely unradiogenic values (0.70077 in samples BBu and BE13 with highest Sr contents of 225 µg/g) to the very radiogenic value of 0.715 (BBm with much lower Sr: 15 µg/g). Other samples range between 0.7064 and 0.7092 (Table 5; Fig. 5a). The Rb contents of the clinopyroxenes are extremely low, close to the detection limit of LA-ICP-MS, and do not support the $^{87}Sr/^{86}Sr$ ratios. They are low enough that no appreciable growth of the low $^{87}Sr/^{86}Sr$ ratios has occurred since

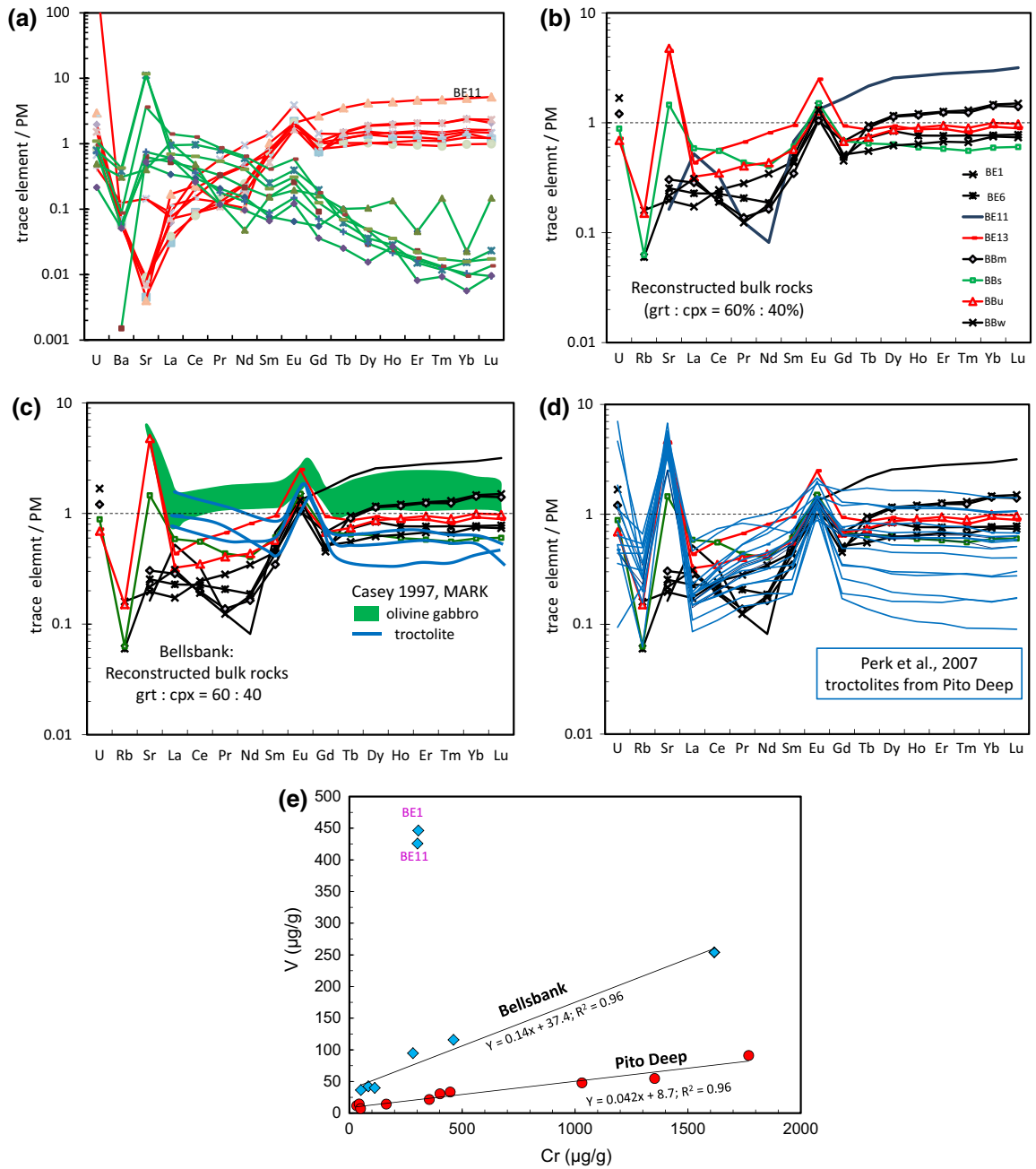

Fig. 3 **a** Extended REE diagrams of garnets and clinopyroxenes from the Bellsbank kyanite/corundum eclogites. **b** Reconstructed bulk rock compositions assuming 60 % modal garnet and 40 % clinopyroxene. **c** Comparison of eclogite trace elements with the troctolites and olivine gabbros from MARK (Kane fracture zone on the Mid-Atlantic ridge; Casey 1997). **d** Comparison with the troctolites from the Pito Deep in the Pacific (Perk et al. 2007). **e** Bulk rock vanadium versus chromium for Bellsbank eclogites and Pito Deep troctolites, with linear regressions giving the slopes of the correlations

the formation of the cpx. High $^{87}Sr/^{86}Sr$ ratios can originate from the equilibration of cpx with a K-bearing phase, but there is no such a phase in the rocks. Four samples were determined as duplicates by solution MC-ICP-MS (from 40 mg separates) and by TIMS (from 2-mg separates). The repeat Sr isotope ratios agree within the respective analytical errors (Table 5), indicating that the picked separates were unlikely to have been significantly contaminated by kimberlite or that secondary cpx was included in the separates. The very unradiogenic $^{87}Sr/^{86}Sr$ values of around 0.70077 correspond to a minimum model age (assuming zero Rb) of about 3.1 Ga (Fig. 5b). Similarly, unradiogenic

Table 4 Oxygen isotope composition ($\delta^{18}O$ ‰) of garnet, primary and secondary clinopyroxene (cpx) and kyanite

Sample	$\delta^{18}O$ ‰ (garnet)	$\delta^{18}O$ ‰ (cpx)	$\delta^{18}O$ ‰ (secondary cpx)	$\delta^{18}O$ ‰ (kyanite)
BE1	3.46	4.57		
BE6	3.77	4.30		
BE11	2.50	2.99		
BE13	4.57	4.86		4.74
BBm	4.40	4.83		
BBs	4.57	4.93		
BBu	2.86	3.48	4.00	
BBw	4.49	5.03		

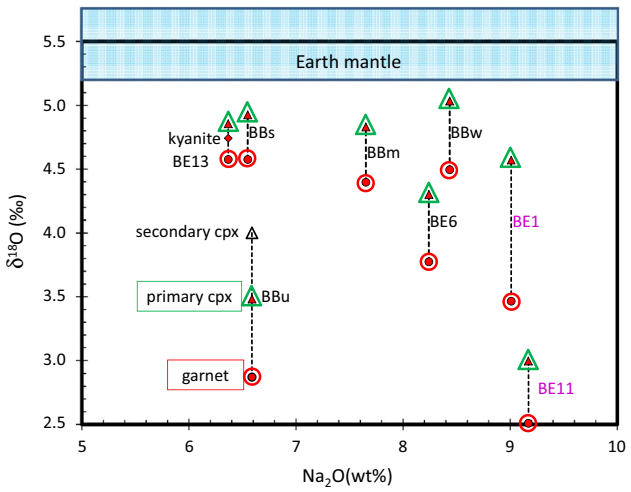

Fig. 4 $\delta^{18}O$ versus Na_2O in the clinopyroxenes. All values are lower than the mantle value of 5.5 ‰. Primary cpx is always higher than coexisting grt

values were reported previously in clinopyroxenes from two Roberts Victor eclogites (Jacob et al. 2005; Gonzaga et al. 2010).

Discussion

The eclogites examined here, with the exception of sample BE11, show perhaps the most pronounced positive Eu anomalies so far analyzed in rocks of direct mantle derivation. These anomalies cannot be made by crystallization of their present modal mineralogy from a magma or by interaction of this assemblage with any known mantle fluid. This and the almost complete overlap of the eclogite trace element patterns of two of our samples with troctolites from MARK and the Pito Deep (Fig. 3c, d) stands as clear evidence that the eclogite protoliths were plagioclase-rich low-pressure cumulates of basaltic magmas that experienced high-temperature seafloor alteration varying extents, to produce $\delta^{18}O$ values lower than the mantle value. High-temperature seafloor alteration adds volatiles to the oceanic crust but leaves the bulk rock chemistry relatively unchanged, as does subsequent dehydration and metamorphism (a general discussion can be found in Jacob 2004). If, subsequently, partial melting in the eclogite stability field occurred, the abundances of the highly incompatible elements are significantly lowered, and the MREE will be fractionated from the HREE (e.g., Fig. 2b), as discussed

Table 5 Sr isotope ratios of clinopyroxenes

Sample	In situ laser data		Calculated from laser data	MC-ICP-MS			TIMS	
	Sr (ppm)	Rb (ppm)	$^{87}Rb/^{86}Sr$	$^{87}Sr/^{86}Sr$	Error (1 s)	$\varepsilon Sr(0)$	$^{87}Sr/^{86}Sr$	Error (1 s)
BE1 cpx	10	0.17	0.049	0.709239	0.000016	60		
BE6 cpx	13	0.03	0.007	0.707139	0.000016	30	0.707744	0.000018
BE11 cpx	8	b.d.l.		0.706862	0.000005	26	0.707995	0.000010
BE13 cpx	221	0.08	0.001	0.700836	0.000005	−59	0.700763	0.000004
BBm cpx	15	b.d.l.		0.715058	0.000006	143		
BBs cpx	72	0.03	0.001	0.706388	0.000007	20		
BBu cpx	233	0.14	0.002	0.700770	0.000003	−60	0.700785	0.000002
BBw cpx	11	0.2	0.050	0.709040	0.000007	57		
std SRM987				0.710239	0.000028 (2 s, $n = 6$)		0.71026	0.00006 (2 s, $n = 3$)

b.d.l. below detection limit

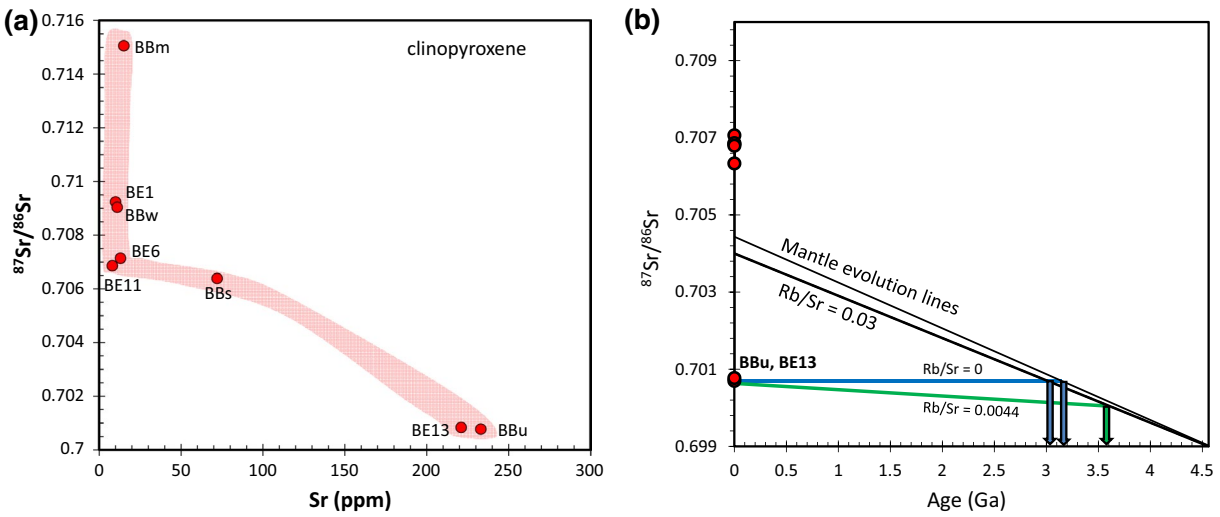

Fig. 5 **a** $^{87}Sr/^{86}Sr$ ratios of the clinopyroxenes versus Sr contents. Two samples have extremely low $^{87}Sr/^{86}Sr$ ratios of around 0.7007. **b** Sr isotope evolution plot illustrating model ages for the least radiogenic clinopyroxenes. These low values correspond to Rb depletion model ages of about 3.2 Ga. If the maximum Rb/Sr ratio of the Pito Deep cumulates (Perk et al. 2007) is taken as a measure of the magmatic Rb/Sr of the eclogite protoliths, we obtain a Rb model age of 3.6 and 3.4 Ga for the average value relative to a mantle with Rb/Sr = 0.03

below. Metasomatic enrichment at any time subsequent to the subduction of the protoliths can only have been minor since only the highly incompatible elements such as La and Ce are noticeably elevated in half of our samples (see Fig. 2b). It appears, however, that these processes exert only minor chemical changes on a number of decisive elements and direct inferences from the present-day compositions can be made for the eclogite protoliths.

Oxygen isotopes: high-temperature seafloor alteration

Modern ocean floor lithologies have $\delta^{18}O$ values that are both lower and higher than the mantle value of 5.5 ± 0.4 ‰ (Muehlenbachs and Clayton 1972; Mattey et al. 1994). Higher $\delta^{18}O$ values than the mantle are due to water–rock exchange at relatively low temperature (McCulloch et al. 1981), while lower values reflect high-temperature seafloor alteration in the lower parts of the oceanic crust. Eclogite and garnet pyroxenite xenoliths worldwide show the same range, and this correspondence is taken as a major argument for a subduction origin of these lithologies (see summary by Jacob 2004). Recently, Huang et al. (2014) questioned the seafloor alteration model for eclogites and proposed that their observed range of the $\delta^{18}O$ values was generated by metasomatism by carbonatitic melts. However, this scenario is effectively ruled out by a detailed study of a metasomatized eclogite made by Riches et al. (2015) who measured invariant, non-mantle like $\delta^{18}O$ values across an eclogite with significant variations in incompatible trace elements. These authors also show, quantitatively, the inability of low-fraction carbonatitic melts to buffer eclogitic wallrocks to the melt $\delta^{18}O$ value. For these reasons, we discuss only the widely accepted paradigm of water–rock exchange in explaining eclogite $\delta^{18}O$ values.

The published $\delta^{18}O$ values of garnets from the Bellsbank eclogites and garnet pyroxenites are all lower than the mantle value (Neal et al. 1990). The low values are consistent with high-temperature alteration in the deeper (plutonic) sections of the ocean floor, where accumulated plagioclase will be prominent. We analyzed both grt and cpx and find that the latter are always higher in $\delta^{18}O$ than grt. Thus, the bulk rock values of four samples are just below the accepted mantle value (Fig. 4) at around 4.8 ‰, indicating detectable, but only minor high-temperature seafloor alteration. This is expected for deep oceanic crustal sections where ingress of circulating ocean water was likely only small. On this basis, we expect that chemical modification of the magmatic protoliths by seawater alteration, such as exchange of Ca and Na, has been only minor.

Major and trace elements: from protoliths to metamorphism

Information on the eclogite protolith composition and its original mineral assemblage may be gained from bulk rock compositions based on chemical analysis or calculated from modal abundances, and from considerations of possible phase relationships at a range of pressures. The former provide only limited information because of the small size and the possibility of contamination and alteration of

the constituent minerals by the host kimberlite. Instead, we consider the metamorphic high-pressure phase relationships of the eclogites in the triangular diagram (Al–Na)–Ca–(Mg + Fe^{total}) and compare them with potential lower pressure phase assemblages (Fig. 1a). Bulk rock compositions lie within the compatibility triangles at the respective pressures. Figure 1a shows that there are two solutions possible for the primary phase assemblage of the eclogites namely (a) a "plagioclase + olivine + Al-bearing clinopyroxene" cumulate at the lowest pressures and (b) a "olivine + spinel + aluminous clinopyroxene" cumulate at elevated pressures. The reasons for this duality lie in the liquidus phase relationships for basaltic systems as shown in the pseudoternary phase diagram fo-di-an (Presnall et al. 1978) at one atmosphere pressure and at elevated pressure (Fig. 6a, c). The comparison of Fig. 6a, b shows that aluminous low-pressure cumulates (upper crustal pressures) from tholeiitic to picritic compositions (red star in Fig. 6a, c) are metamorphosed to (coesite) kyanite grospydites (coesite) kyanite eclogites and bimineralic eclogites, while intermediate (<7 GPa) pressure cumulates are metamorphosed to kyanite eclogites, corundum eclogites, alkremites, and garnet pyroxenites (Fig. 6c, d). These relationships are elaborated further below.

Olivine tholeiitic to picritic melts (red star in Fig. 6a) precipitate at low pressures first olivine to form dunites, then ol + plag to form troctolites and anorthositic rocks (leucotroctolites) and, when cpx joins the assemblage, olivine gabbros (Fig. 6a, b). The resulting plagioclase-rich cumulates all have pronounced positive Eu anomalies (inserts in Fig. 6a) together with striking positive Sr anomalies. The late crystallizing cpx will have a negative Eu anomaly. These trace element signatures can be found in the plutonic sections of the present-day oceanic crust, in ophiolites such as in Oman and in large igneous intrusions like the Bushveld complex.

High-pressure metamorphism changes these low-pressure assemblages to (quartz/coesite)–kyanite–grospydites, (quartz, coesite)–kyanite eclogites and bimineralic eclogites. This is indicated in Fig. 6b by hypothetical phase compatibility triangles and fields, in which the field for coesite–kyanite eclogites corresponds to the range of the compatibility triangles for the Bellsbank eclogites (compare Fig. 1). The compositions of metamorphic minerals vary for a given bulk composition as a function of *P* and *T* and their phase compatibility triangles shift accordingly. To trace the likely phase transformations and resulting lithological variability in real rocks, we have plotted the compositions of dunitic and anorthositic troctolites, troctolites, and ol-gabbros from the Pito Deep (Perk et al. 2007) and of a selection of such rocks from the MARK area (Casey 1997) into Fig. 6b. Many of these oceanic rocks plot parallel to but slightly offset from the ol-an join and extend toward aluminous cpx from the troctolitic compositions, tracking the compositional range of the Bellsbank eclogites. Phase relationships show that metamorphism in the eclogite stability field transforms anorthositic troctolites into (quartz-/coesite-bearing) kyanite grospydites, whereas the troctolites and dunitic troctolites plus some of the ol-gabbros become (quartz/coesite) kyanite eclogites (Fig. 6b). The more dunitic troctolites and olivine gabbros metamorphize to bimineralic eclogites. The overlap between the field for the cumulates and the red field (range of the compatibility triangles of the Bellsbank eclogites) gives the possible parental compositions for the latter. It is clear from such metamorphic transitions that the higher pressure phase assemblages must inherit the trace element compositional characteristics of their protoliths, most significantly the relatively flat middle to heavy REE patterns that are accompanied by prominent positive Eu and Sr anomalies reflecting their plagioclase-rich parentage.

At elevated pressures, the liquidus fields of spinel and diopside expand in the pseudoternary di-fo-an system (Presnall et al. 1978), and the fields of ol and plag become separated (compare Fig. 6a with Fig. 6c). Also, orthopyroxene will eventually become stable (e.g., Green and Ringwood 1967), and the phases crystallizing from tholeiitic to picritic melts will be ol, (ol + opx), ol (+opx) + sp, ol (+opx) + sp + cpx, (opx) + cpx + sp, and eventually cpx + sp + plag, and corresponding cumulates will be formed. The low-pressure phase compatibility triangle ol-plag-cpx is replaced by (ol, opx)-sp-aluminous cpx at the higher pressures. The probable range of bulk rock compositions of the cumulates is indicated in Fig. 6d as tilted squares. These compositions would be manifest at low pressure as dunites, harzburgites, sp-harzburgites, sp-wehrlites and sp-pyroxenites, and finally gabbros. Within these parental assemblages, a positive Eu anomaly can appear only in the cumulates of highly differentiated magmas (see inserts in Fig. 6c) since plagioclase crystallization occurs only very late. The wehrlitic and pyroxenitic cumulates are high in Al_2O_3 because of accumulated spinel and very aluminous clinopyroxene and orthopyroxene (e.g., Green and Ringwood 1967; Freise et al. 2009). These low-pressure crystallization products are metamorphosed to aluminous garnet harzburgites, alkremites (=garnet–spinel rocks with small amounts of corundum, e.g., Nixon et al. 1978), (coesite) kyanite eclogites and garnet pyroxenites in the eclogite stability field. Such an origin neatly explains the origin of the enigmatic highly aluminous alkremites which cannot crystallize as garnet–spinel assemblages at higher pressure from any known natural melt composition. One of our samples (BE11) has appreciable amounts of corundum, but only a hint of a positive Eu anomaly (if any). This sample also has higher middle to heavy REE contents, a more steeply sloping middle to heavy REE pattern and the most

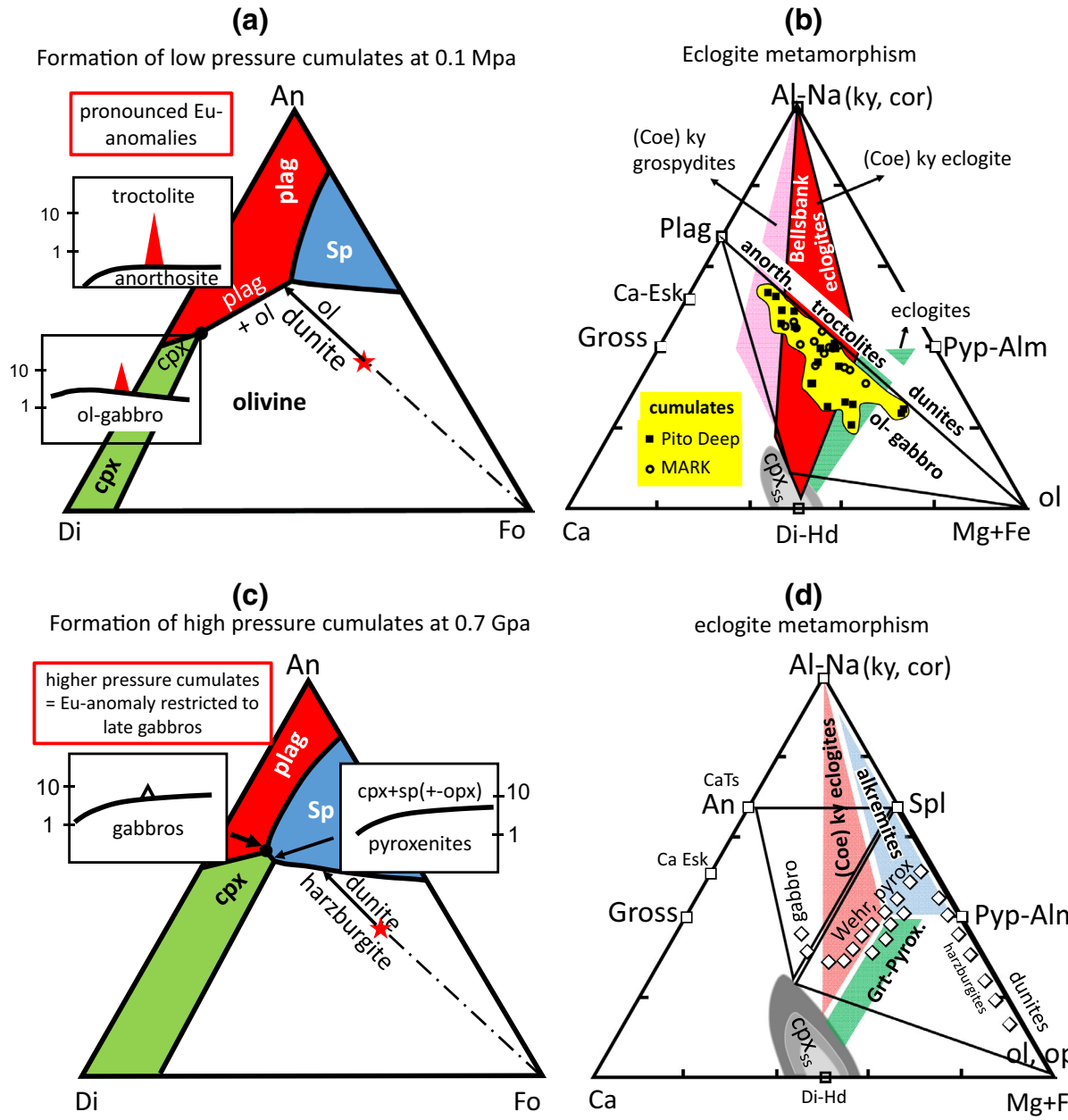

Fig. 6 **a** Liquidus phase diagram for the pseudoternary system An-Di-Fo at 1 atm after Presnall et al. (1978). Olivine, olivine + plagioclase, and finally olivine + plagioclase + clinopyroxene are the liquidus phases for tholeiitic to picritic magmas (*red star*). The pronounced Eu anomalies of such cumulates are emphasized. **b** The compositions of cumulates from the Pito Deep and the Kane fracture zone (MARK) plotted into the (Al–Na)–Ca–(Mg + Fe) triangle. They plot within the compatibility triangle ol-An-(Di-Hd). The Al solubility in cpx is indicated schematically by the *gray areas* (for different temperatures). The cumulates are troctolitic dunites, troctolites, anorthositic troctolites, and ol-gabbros. These are metamorphosed at high pressures to (coesite) kyanite grospydites, (coesite) kyanite eclogites, and bimineralic eclogites as shown schematically in the Figure. Instead of a schematic field for (coesite) kyanite eclogites, we have combined the actual range of the compatibility triangles for Bellsbank into the red field. The overlap between this field and the field for the cumulates gives the possible parental compositions for the Bellsbank eclogites. A SiO_2 polymorph (coesite) occurs in the lower pressure range of the experiments (compared to the natural rocks). Coesite is reacted out at higher pressures as described in Fig. 5 below. **c** Liquidus phase diagram at 0.7 GPa after Presnall et al. (1978). Ol(± opx), ol(± opx) + sp, ol(± opx) + sp + cpx, and finally sp + cpx + plag are the liquidus phases at the higher pressure. In this evolution, a Eu anomaly would be restricted to the late crystallizing gabbros. **d** Phase triangle ol-An-(Di-Hd): two compatibility triangles are applicable: ol(± opx) + sp + aluminous cpx and sp + aluminous cpx + plag. Al solubility in cpx is increased at the higher pressures and temperatures as indicated schematically by the *dark gray area*. Hypothetical cumulate compositions (*black-rimmed squares*) range from dunites and harzburgites to wehrlites and pyroxenites. These are metamorphosed at high pressures to alkremites, (coesite) kyanite eclogites and grt-pyroxenites as shown schematically in the figure

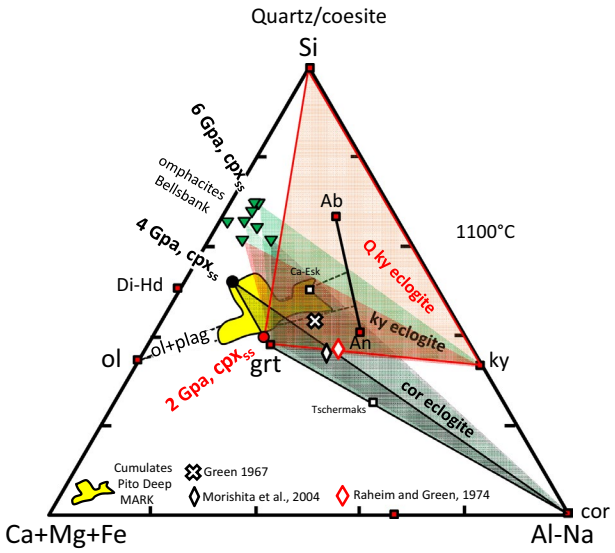

Fig. 7 Section through the Ca–(Mg + Fe)–(Al–Na)–Si tetrahedron at Ca:(Mg + Fe) = 50:50 showing the compositions of experimental starting materials from Morishita et al. (2004), a lunar highland basalt (*red diamond*; Råheim and Green, 1974) and a kyanite eclogite (*black cross*; Green 1967), the phase compatibility triangles for experiments at 2 and 4 GPa and 1100 °C and several compatibility triangles for the Bellsbank eclogites from 4 to 6 GPa. The *yellow field* is the compositional range of the cumulates from the Pito Deep and the Kane Fracture Zone (MARK). Garnets plot onto one point, but the plagioclase compositions can be represented separately. The clinopyroxenes vary widely in composition because the various possible Al components Ca-Tschermaks, Ca-Eskola, and jadeite vary with pressure and temperature. This determines the coexistence of a SiO_2 phase with kyanite via the reaction $CaAl_2SiO_6 + SiO_2 = Al_2SiO_5 + CaSiO_3$. The tie line cpx_{ss} kyanite rotates with increasing pressure (decreasing temperature) toward the Si apex so that most Pito and MARK cumulates would crystallize to quartz/coesite–kyanite eclogites at the lower pressures and to kyanite only eclogites at higher pressures

depleted LREE contents than all other samples (Fig. 2b). These features are consistent with a higher pressure origin of its protolith as a cumulate of (ol, opx) + spinel + Al-rich pyroxene.

The clinopyroxenes in two samples (BE13 and BBu) contain a Ca-Eskola component, indicating a SiO_2 activity near one in the rocks. This observation is significant because a silica polymorph occurs at pressures between 2 and 3.6 GPa together with kyanite in the experiments of Råheim and Green (1974) and Green (1967). They define, from an experimental view point, the phase assemblage produced during eclogite-facies metamorphism of high-Al basaltic compositions or Al-rich cumulates. Figure 7 is a section through the Ca–(Mg + Fe)–(Al–Na)–Si tetrahedron at Ca:(Mg + Fe) = 50:50 for temperatures at around 1100 °C and varying pressures. It shows the compositions of the experimental starting materials and phase compatibility triangles for experiments at 2 and 4 GPa along with several phase compatibility triangles for the Bellsbank eclogites. Garnets plot in this diagram at a single point, but the spectrum of plagioclase compositions can be displayed. Clinopyroxene compositions (cpx_{ss}) vary widely depending on their Ca, Mg Tschermaks-, Ca-Eskola-, and jadeite components which depend on pressure, temperature, and bulk rock composition. It can be seen from Fig. 7 that a silica polymorph can coexist with kyanite when the bulk rock composition lies on the Si-rich side of the cpx_{ss}-ky tie line. This tie line rotates with increasing pressure (decreasing temperature) toward the Si apex due to the reaction $CaAl_2SiO_6 + SiO_2 = Al_2SiO_5 + CaSiO_3$. Bulk rock compositions such as most of the plagioclase-rich cumulates from the Pito Deep and the Kane fracture zone (yellow field in Fig. 7) and the kyanite eclogite of Green (1967; black cross) would crystallize as (quartz)–coesite–kyanite eclogites but may loose the SiO_2 phase at the highest pressures and become kyanite eclogites only. Kyanite alone coexists with grt and cpx for compositions below the cpx_{ss}-ky tie line and above the grt-ky tie line. Corundum crystallizes for compositions below this tie line because of the reaction grt + ky = cpx_{ss} + cor. Corundum eclogites are stabilized to higher pressures as well because of the changing composition of cpx. Partial melting in the eclogite stability field is a more direct way to lower the SiO_2 activity and content by a change in the bulk rock composition. Increasing pressure shifts the cpx-ky and the grt-ky tie lines toward the SiO_2 apex, and increasing partial melting shifts the composition of the residues below these tie lines, where first quartz/coesite and then kyanite are eliminated. The rocks will become kyanite, kyanite + corundum, and finally corundum eclogites.

The detailed effects of partial melting will be discussed further below after the following discussion on the similarities and dissimilarities between the eclogites and the troctolites from the Kane fracture zone (MARK) and the Pito Deep. Samples BE13, BBu, and BBs (red and green patterns in Figs. 3, A4) have flat middle to heavy REE patterns, mirroring the compositions of the troctolites from MARK, from the Pito Deep, and from the Oman ophiolite (Figs. 3c, d, A4a). The similarities of BE13 and BBu with many Pito Deep troctolites extend to LREE depletion, Sr contents, and magnitudes of the Eu anomalies (Fig. 3d). This may mean that the parental melts were originally LREE depleted like MORB, i.e., the cumulates inherited this signature from a depleted mantle source. The chemical compositions of the other eclogites are modified by partial melting in the eclogite stability field (increased LREE depletion, fractionation of MREE from HREE, decreased Sr contents) and by metasomatism of the most incompatible elements (see below).

The troctolites from MARK and the troctolites from the Pito Deep with the higher REE contents and smaller Eu anomalies (Fig. 3c, d) are cumulates from more evolved

melts because their olivines and plagioclases have compositions around Fo_{80}, respectively, An_{70} (Fig. 2a, b). The major elements of the eclogites should be in the same range as those of the intermediate cumulates if the parental magmas were similar, and these compositions should reflect those of the original olivines and plagioclases. The overlap is very good in SiO_2, CaO, and Al_2O_3 (Figs. 2a, A2c), but Na_2O is higher (Fig. 2b) as well as FeO (Fig. A2b).

The high Na_2O contents of the eclogites are reflected by 5–12 % nepheline in the CIPW norm (Table A2) while only few of the Pito Deep cumulates are nepheline-normative (all Fe taken as FeO) and most hypersthene-normative as common for MORB. The cause of the relatively high Na_2O contents may be that the parental magmas were more alkali-rich than MORB because they originate from a less depleted mantle and/or because they originated at greater depths than MORB due to the higher mantle potential temperatures in the Archean, e.g., as alkali-picrites (Green, 2015). The normative plagioclase content (with ~An_{80}) is around 50 % and of diopside and olivine between 15 and 25 % each. The Mg values are lower than in the MARK and Pito Deep cumulates and between 65 and 75, whereas the Ni contents are the same or higher up to 750 µg/g (Fig. 2c). They are in fact far too high in relation to Mg#. A possible and plausible solution is that the cumulates stem from sulfur-saturated magmas and that immiscible sulfide melt droplets accumulated together with olivine and plagioclase. The Mg value of the silicate portion then becomes elevated, e.g., in sample BBu from 71 to 78 if 2 wt% FeO (absolute) is subtracted as the amount corresponding to an immiscible sulfide melt. Accumulating sulfide melt droplets increase the Ni content of a bulk rock quickly because of the very high partition coefficient of Ni into sulfide melts (e.g., Rajamani and Naldrett 2006). It appears that the protoliths of the ky/cor eclogites were plagioclase-rich cumulates like the troctolites from Mark and the Pito Deep, but that the parental magmas were sulfide-saturated and more alkali-rich than MORB.

Reduced Archean mantle melts: Eu anomalies and V/Cr ratios

The strong positive Eu anomalies of the Bellsbank mantle eclogites and the interpretation as plagioclase-rich cumulates potentially may constrain the oxygen fugacity of their original magma via the partitioning of Eu between plagioclase and melt (Drake and Weill 1975; Laubier et al. 2014). However, the application of this oxybarometer is hampered by the lack of information on the Eu content of the melt. We can assume the parental melt had the average Eu content of modern MORB (1.22 µg/g; Arevalo and McDonough 2010), and that the middle to heavy REE of the calculated bulk rocks were all contained in the original plagioclase neglecting clinopyroxene. We used the Eu anomaly and the REE contents of the calculated bulk rock of sample BBu and the formulations of Aigner-Torres et al. (2007; equations 2 and 5) to derive a value for an oxygen fugacity. We also used the averaged partition coefficients for Sm, Gd, and Sr from their experiments to derive D^{Eu3+} and D^{Eu2+}. We obtained a range of values from $\Delta FMQ = -3.5$ and $\Delta FMQ = +0.3$ depending on the assumed value for the "reducibility" (susceptibility to reduction) in their equation (5). The ΔFMQ values range from significantly more reducing to similar values as for modern MORB ($\Delta FMQ = 0$; Lee et al. 2005; Perk et al. 2007). However, these estimates for the Bellsbank eclogites are highly dependent on the unknown amount and concentration of REE in cpx and its effect on lowering the bulk rock-positive Eu anomaly due to its coexisting negative anomaly.

An alternative to using Eu is to employ bulk rock V/Sc ratios to estimate oxygen fugacity (e.g., Canil 1999). The principle of the method is to use the ratio of two elements for which the solid–melt partitioning is strongly dependent on oxygen fugacity for one element and not for the other, and Mallmann and O'Neill (2009) calibrated the partitioning of many elements that could be selected as such pairs. Applying this approach to a range of basaltic rocks, Li and Lee (2004) found evidence that the Archean mantle fO_2 was similar to that of the present day, a conclusion in apparent conflict with the observation that the evolution of oxygen abundance in the Earth's atmosphere requires a more reduced mantle in the Archean (Kasting et al. 1993). The latter conclusion is supported by the study of Aulbach and Viljoen (2015) who determined more reducing conditions for the Archean, by two log units compared to MORB, through application of the V/Sc method to Archean eclogite xenoliths.

The V/Sc method can be used for cumulates, ideally in a situation where both elements are contained in only one of the crystallizing phases. For V and Sc in plag-ol-cpx cumulates, the ratio of the heterovalent vanadium to monovalent Sc would be higher in cumulates from more reduced melts compared to those from more oxidized melts. Examining the Pito Deep troctolites and the Bellsbank eclogites, we find good correlations between V and Sc, with a slope of 3.2 for the Pito Deep and 5.8 for the five Bellsbank eclogites late stage where partial melting is minimal or absent (see below). The V/Sc ratio is clearly higher in the Bellsbank eclogites than in the Pito Deep troctolites. This result is a further indication that Archean magmas were more reduced than modern MORB. However, because Sc preferentially partitions into cpx, which is generally an intercumulus phase, we feel that some caution should be used in applying bulk rock V/Sc ratios to estimate parental melt fO_2 in cumulate rocks.

Another element pair with contrasting redox response is V and Cr. Both these elements can be contained in the early crystallizing phase olivine. The $D_{Cr}^{ol/l}$ is independent of the oxygen fugacity over a wide range and can be used in an analogous way to Sc while $D_{V}^{ol/l}$ depends strongly on fO_2 (e.g., Gaetani and Grove 1997; Mallmann and O'Neill 2009). The bulk rock V/Cr ratios of the eclogitic counterparts of the ol-plag(-cpx) cumulates will dominantly reflect the precursor cumulate olivine, allowing estimation of the oxygen fugacity of the parent melt. We have already shown in Fig. 3e that the V/Cr ratio correlates in six Bellsbank eclogites, with a significantly higher slope (=0.14) than in the troctolites from the Pito Deep (=0.04). This relationship indicates that the parental magmas that formed the low-pressure cumulate precursors to the Bellsbank eclogites were more reduced than modern MORB magmas (Fig. 3e).

Quantitative estimation of oxygen fugacities can be made using the experimental data of Mallmann and O'Neill (2009; Fig. 8). The partitioning of V and Cr between ol-melt and cpx-melt is reproduced in Fig. 8 for their starting materials V1, VS1, and V7. Values for $Dv^{ol/l}$, $Dv^{cpx/l}$, and $D_{Cr}^{cpx/l}$, at a chosen oxygen fugacity, can be taken from Mallmann and O'Neill (2009). Using their value for $D_{Cr}^{ol/l}$ of 0.85 and assuming all V and Cr to be hosted in olivine, the $D_{V}^{ol/l}$ values for the Pito Deep can be derived as V/Cr × 0.85 = 0.36 and for Bellsbank as V/Cr × 0.85 = 0.119. The resulting values give oxygen fugacities as log fO_2 = −8 and −10 (Fig. 8). The same exercise can be performed assuming that all V and Cr are contained in cpx. The oxygen fugacities are shifted to less reducing values but the relative differences remain. A potential correction for the effect of cpx lies along the connection lines between the ol and cpx values, and the solid white symbols in Fig. 8 illustrate such a correction for 20 to 30 % cpx. Applying this "correction," the oxygen fugacity for the Pito Deep cumulates becomes ΔFMQ = ~0, as for modern MORB and gives ΔFMQ = −2 for the Archean Bellsbank eclogites. On this basis, the Archean mantle appears to be more reducing than the present-day mantle, supporting the inference of Aulbach and Viljoen (2015) made from V/Sc ratios in eclogites that likely were original melt compositions.

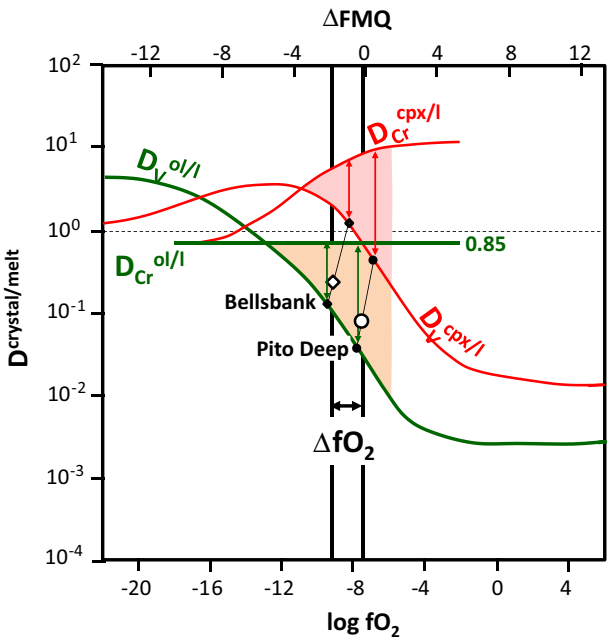

Fig. 8 Partition coefficients for V and Cr between ol/l and cpx/l as a function of fO_2 reproduced from the diagrams in Mallmann and O'Neill (2009). The positions for Bellsbank and the Pito Deep samples are deduced from the slopes of the V and Cr correlations in Fig. 3e (see text)

The assumption that all V and Cr in the Bellsbank eclogites were originally mainly in olivine is not correct if immiscible sulfide droplets accumulated together with ol and plag, as we invoked to explain the Fe- and Ni-rich nature of the Bellsbank cumulates. Gaetani and Grove (1997) showed that sulfide would contain V and Cr but with a constant K_D ratio of about 0.25 over a wide range of oxygen fugacities. The V/Cr ratio of the Bellsbank eclogites would then reflect the combined partitioning of these elements into the low-pressure olivine and sulfide cumulate phases, prior to eclogite-facies metamorphism. This would mean that V/Cr of olivine alone is higher than that of the bulk rock (silicates + sulfides), and estimated oxygen fugacities would be even lower. Gaetani and Grove (1997) also provide olivine/silicate melt partition coefficients for V and Cr as a function of ($\log fS_2^{1/2} - \log fO_2^{1/2}$). A straight comparison of V/Cr ratios of the Pito Deep troctolites and the eclogites on this basis indicates that fO_2 for the Pito Deep cumulates is somewhat above ΔFMQ = 0 and ΔFMQ = −2 for the Bellsbank eclogites. Hence, even accounting for the uncertainties involved in our various assumptions, it is hard to escape the conclusion that the Archean magmas that formed the precursor cumulates to the Bellsbank eclogites were significantly more reduced than those that form cumulates in modern mid-ocean ridge settings.

Partial melting in the eclogite stability field and metasomatism

Five of the Bellsbank eclogite samples have only weak Sr anomalies (Fig. 3b) but are strongly depleted in Nd and Pr, have positively sloped middle to heavy REE patterns, and are re-enriched in Ce and La. These features, along with the absence of an SiO_2 phase, are the signatures of partial melting in the eclogite stability field, followed by a later metasomatic overprint. We have carried out calculations for fractional partial melting in the eclogite stability field using the

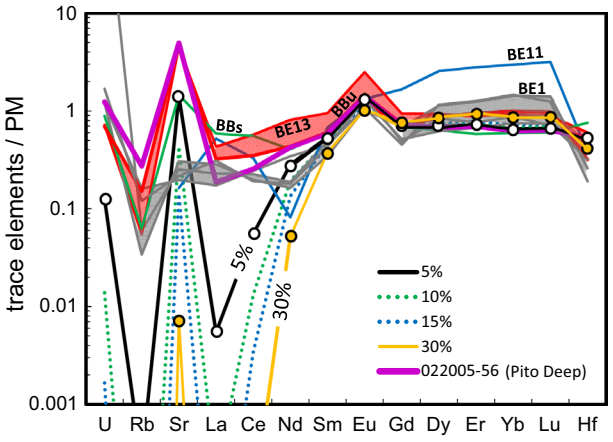

Fig. 9 Trace element compositions of residues from various degrees of fractional partial melting in the eclogite stability field using a troctolite from the Pito Deep as parental rock and the trace element partition coefficients of Green et al. (2000). Fields of eclogites are summarized for comparison, i.e., BBu and BE13 as *red field*, indicating no partial melting and a *gray field* for samples that experienced intermediate degrees of partial melting

partition coefficients of Green et al. (2000), a grt:cpx ratio of 60:40 in the bulk rock and a 50:50 ratio as a contribution to the melt. The results are shown for the residues in Fig. 9. We have performed these calculations using a range of Pito Deep troctolites as parental material, but highlight the results for Pito Deep sample 022005-56 because of its strong similarities with sample Bellsbank eclogite BBu. The LREE and Rb concentrations are dramatically lowered with increasing degrees of partial melting. Concentrations of Sr and U decrease less rapidly, while the middle to heavy REE increase with the degree of partial melting. Comparison of the Sm/Nd ratios (i.e., their degree of LREE depletion) indicates that no partial melting affects samples BE13 and BBu, whereas other samples have experienced between 5 and 30 %. Strontium is lowered to the present-day measured values of ~0.2 × PM or below, in the samples that experienced intermediate degrees of partial melting and is much lower in those affected by 30 % partial melting. These values are lowered even further, to 0.6–2 μg/g Sr in the residue when the Sr partition coefficients (0.055 compared to 0.5) of Pertermann et al. (2004) are used. If metasomatic re-enrichment occurred, as indicated by increased La and Ce abundances, these low Sr and LREE concentrations are overwhelmed by the metasomatic agent, and hence their present measured concentrations simply reflect the composition of the metasomatizing agent.

Extremely unradiogenic Sr isotope ratios: Meso-Archean partial melting

Considerable effort has been devoted to determining the "age" of eclogites by using various radiometric dating methods, and yet, this remains a challenging problem. Most authors interpreted the ancient ages obtained from multi-point mineral and whole-rock isochrons or model ages as reflecting the age of emplacement of the eclogites into the lithospheric mantle (e.g., Jagoutz 1988; Jacob and Foley 1999; Pearson and Nowell 2002; Heaman et al. 2006) while others have considered some of the ages as representing the age of the basaltic protolith (Pearson et al. 1995; Menzies et al. 2003; Jacob et al. 2005; Schmidberger et al. 2007). The most extensive data set for attempting to constrain the age of these rocks using the isochron approach exists as grt-cpx tie lines using, predominantly the Lu–Hf and Sm–Nd systems. Recently, Shu et al. (2014) discussed the interpretation of these "isochrons" and concluded that they either reflect closure ages in a steadily cooling mantle or kimberlite eruption ages but do not give age information on the protolith or on metamorphism.

Sr isotopes have been relatively under-used since the early attempts by Macgregor and Manton (1986) to determine eclogite ages. Jacob et al. (2005) and Gonzaga et al. (2010) measured very low $^{87}Sr/^{86}Sr$ ratios in cpx of two Roberts Victor eclogites that correspond to a model age of around 3 Ga. They suggested that such values may date the age of eclogites but did not elaborate any further on the geological meaning. The clinopyroxenes in two of our samples (BE13 and BBu) have also extremely unradiogenic $^{87}Sr/^{86}Sr$ ratios (0.70076 and 0.70079) together with very low Rb/Sr ratios (0.0004 and 0.0006) but high Sr contents (Table 5). The low $^{87}Sr/^{86}Sr$ ratios mark the minimum time when Rb was effectively removed from the rocks probably by partial melting in the eclogite stability field or by dehydration during subduction. A projection of the $^{87}Sr/^{86}Sr$ ratios to the mantle evolution line gives model ages between 3.0 to 3.2 Ga (Fig. 5b). This is a minimum age for the time of partial melting because the original cumulates must have had at least 10 times higher Rb/Sr ratios than the present-day rocks based on the Rb/Sr ratios of the gabbroic to troctolitic cumulates from the Pito Deep [average 0.002 ($n = 11$), maximum 0.0044; Perk et al. 2007]. The Rb contents of these cumulates appear to be primary because the Rb/Sr ratios of magmatic plagioclases are around 0.015 as can be deduced from the partition coefficients given by Tepley et al. (2010).

Depending on the time span between fractional crystallization and dehydration or partial melting in the eclogite stability field, the $^{87}Sr/^{86}Sr$ ratios could evolve in the ocean floor residence stage or the eclogite stage, to varying extents. The projection of the measured Sr isotope compositions onto the mantle evolution line (Fig. 5b) therefore leads to minimum ages, especially for the time of the original low-pressure partial melting in the mantle. We have used the Rb/Sr ratios of the Pito Deep cumulates as a guide to the magmatic Rb/Sr ratios of the eclogite protoliths and

calculated Rb–Sr model ages for Earth's mantle with Rb/Sr ratio = 0.03. Assuming an Rb/Sr ratio of zero—the most conservative approach—gives a model age of 3.0 Ga, whereas a more realistic Rb/Sr ratio of 0.002 (the average Rb/Sr ratio of the Pito cumulates) gives a model age of 3.4 Ga (Fig. 5b). This model age may approximate to the age of shallow partial melting in the mantle and fractional crystallization within the oceanic crust; yet, it may still be a minimum age considering the Rb/Sr equilibrium partitioning of plagioclase. The low Sr isotope ratios of samples BE13 and BBu, and their trace element contents and patterns indicate that the original cumulate bulk rock composition was largely preserved throughout the complex history of the rocks (except for the most incompatible elements).

The other six Bellsbank eclogites have much more radiogenic $^{87}Sr/^{86}Sr$ ratios, varying from 0.706 to 0.715, that are unsupported by their present-day Rb/Sr ratios. This indicates a more complex evolution for the Rb–Sr system in these rocks. Consideration of their trace element systematics indicates that all of these eclogites experienced varying degrees of partial melting, loosing most of their original Sr inventory during this process (see above). They were subsequently overprinted with small amounts of a metasomatic agent from a source with high Rb/Sr ratios and that had sufficient time to develop high to very high $^{87}Sr/^{86}Sr$ ratios. A Rb/Sr ratio of 1.86 for example would lead to an increase in $^{87}Sr/^{86}Sr$ ratios from 0.7007 to 0.715 within 200 Ma. These ratios are very high but can be found in pelitic sediments, likely to be subducted along with oceanic crust. Whatever the source of the much more radiogenic Sr isotopes, a crude correlation between $^{87}Sr/^{86}Sr$ and 1/Sr is indicative of mixing/addition influencing the Sr isotopic composition of these rocks. We cannot entirely exclude the possibility of contamination/overprinting of very low original Sr by the host Bellsbank kimberlite magma because the $^{87}Sr/^{86}Sr$ ratios of the clinopyroxenes from four samples lie within the Group 2 kimberlite field (Nowell et al. 2004). We consider this possibility as unlikely because of the short time span between the entrainment in the magma and kimberlite eruption.

Post-Archean analogues of aluminous cratonic eclogites

Corundum-bearing mafic layers with positive Eu anomalies have been described from three peridotite massifs: Beni Bousera in Morocco (Kornprobst et al. 1989), the Ronda massif in Spain (Morishita and Arai 2001), and the Horoman peridotite in Japan (Morishita et al. 2004). The age for pyroxenites in these massifs has been estimated to be Mesoproterozoic (e.g., Pearson and Nowell 2004). These aluminous mantle-derived rocks have long been interpreted as originating as metamorphosed plagioclase-rich cumulates (e.g., Kornprobst et al. 1989). They have positive Eu and Sr anomalies, flat middle to heavy REE patterns, and LREE depletion, in common with the Bellsbank eclogites (electronic appendix Figs. A4 b and c). The abundances of the middle to heavy REE are similar (Beni Bousera) to our eclogites or lower (Horoman, Ronda). This variation can be explained by varying amounts of olivine settling in the original cumulates. The positive Eu and Sr anomalies are highest at Ronda and the middle to heavy REE abundances lowest, indicating that these rocks were originally the most olivine-rich cumulates, likely containing very anorthite-rich plagioclase. These aluminous pyroxenite layers are the more recent record of the subduction of ocean floor cumulates emplaced within ultramafic massifs.

Summary and outlook

Kyanite-/corundum-bearing eclogites from the Bellsbank kimberlite originate from depths between 150 and 200 km, indicating that these lithologies are spread throughout the lower part of the cratonic mantle root. Despite their high-pressure equilibration, their aluminous compositions, striking positive Eu anomalies, flat middle and heavy REE patterns, they retain clear signatures of the low-pressure origin of their precursor rocks, such as REE abundances and $\delta^{18}O$ values lower than the Earth's mantle. The eclogites have incompatible trace element compositions similar to present-day ocean floor and ophiolite troctolites that evolved from tholeiitic to picritic melts at low to moderate pressure in the oceanic crust. This complex evolution of the eclogites, from protolith to current high-pressure mineralogy, is summarized schematically in Fig. 10.

Bellsbank aluminous eclogite evolution involves partial melting at low pressure of a reduced mantle to form the original melts, subsequent fractional crystallization of these melts dominated by plagioclase and olivine plus some immiscible sulfide melt, of seafloor alteration of the cumulates, subduction into the mantle, eclogitization, and finally partial melting that began and ended more than ~3.2 Ga ago. This is the minimum age indicated by the very low $^{87}Sr/^{86}Sr$ isotope ratios in clinopyroxenes of two samples. The only significant change to these rocks since the Mid-Archean probably was a slow adjustment of the mineral compositions to decreasing temperatures during the cooling of the subcratonic mantle (at a rate of about 0.1 °C/Ma; Shu et al. 2014).

The original partial melting event that produced the parental magmas occurred in a mid-ocean ridge setting where picritic to tholeiitic melts were generated from an already LREE depleted mantle (deduced from the extended REE patterns of the eclogites that coincide with modern-day ocean floor cumulates such as those from MARK and

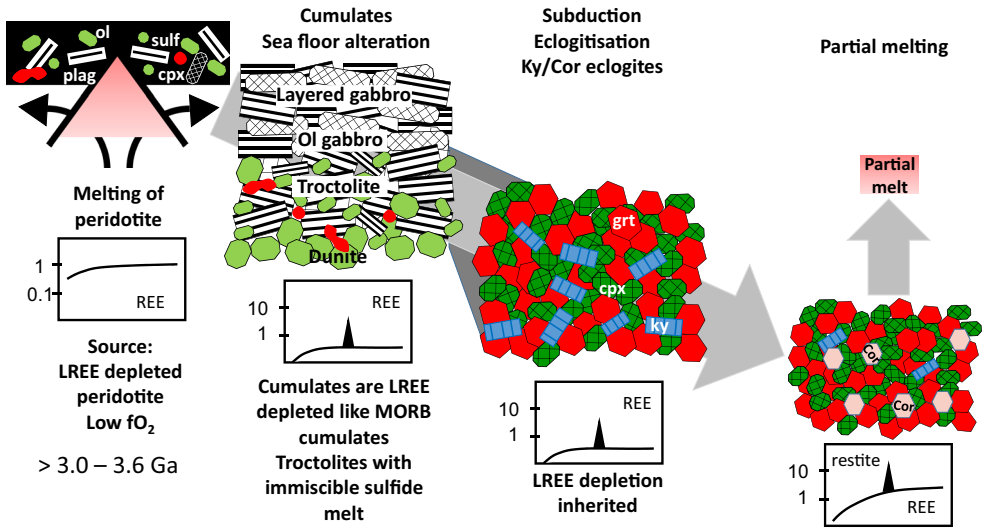

Fig. 10 Schematic representation of the genesis and geologic history of Bellsbank kyanite/corundum eclogites with substantial positive Eu and Sr anomalies. Dunites, troctolites, and gabbros accumulated in the plutonic section and were subducted into the eclogite stability field. Our samples dominantly comprise the troctolitic to gabbroic section which was altered to various extents at high temperatures in deep-seated fracture zones. Subduction progressed to beyond 4 GPa where kyanite eclogites crystallized from the aluminous crustal protoliths. Quartz/coesite is reacted out at this pressure due to the reaction grt + SiO_2 = cpx + kyanite. Variable partial melting and the loss of a Si-rich melt generated corundum in the residue. Subsequent cooling over 3 Ga to the ambient mantle temperatures prior to eruption in a kimberlite 120 Ma ago led to an increase in the modal abundances of kyanite and corundum and concomitant changes in the chemical compositions of grt and cpx

the Pito Deep; Fig. 3c, d). V/Cr systematics indicate that these magmas were more reduced than the present-day oceanic basalts, but were richer Na possibly corresponding to alkali-picrites and were sulfur saturated producing troctolites with pronounced Eu anomalies. Hydrothermal alteration in the plutonic section of the ocean floor affected oxygen isotopes to various extents, possibly introducing Na_2O, but had otherwise little affecting the chemistry of the rocks. Two samples retained their original very unradiogenic Sr isotopic ratios, more or less unchanged to the present day. Subduction followed, to conditions where quartz/coesite was reacted out, either by high-pressure reaction or by partial melting, or a combination of both processes, leaving kyanite-bearing and eventually corundum eclogite as a residue. The effects of partial melting are documented in the higher temperature samples by positively inclined middle to heavy REE patterns and by a strong depletion of the LREE. All these processes were completed before 3.2 Ga. Cooling within stable cratonic lithosphere led to an increase in the modal abundances of kyanite and/or corundum and garnet and a concomitant change in the chemical composition of grt and cpx.

The origin of the majority of the eclogites described here can be attributed to very low-pressure accumulation in a setting analogous to today's mid-ocean ridge settings. However, sample BE11 requires an origin as cumulate at elevated pressures where crustal thickness was 20 km or more. This is feasible considering the probable Early Archean age of the samples. A cumulative origin at elevated crustal pressures may be the explanation for the protoliths of rare eclogite-facies xenoliths such as alkremites. The proposed oceanic crustal origin of these aluminous eclogites completes the tectonic picture revealed by the entire suite of eclogite-facies rocks residing in cratonic mantle lithosphere and removes any doubt of their low-pressure heritage.

The Rb–Sr model age of 3.2 Ga is a minimum, calculated assuming an Rb/Sr ratio of zero. It approximates the age of the last effective removal of Rb from the rock either by dehydration during subduction or by partial melting. The time of primary melt generation from the mantle, i.e., the generation of oceanic crust, must have been earlier and possibly in the Early Archean since the oldest crustal age from the Kaapvaal craton is 3.6 Ga. Because of the striking similarity of the geochemical features of the ky/cor eclogites with cumulates of the modern-day oceanic crust, we can postulate that the magmatic and subduction processes driving modern plate tectonics already existed in at least the Mid-Archean and possibly the Early Archean.

Acknowledgments The authors profited from the continuous help and support in the laboratory, in the field, and through discussions by A. Gerdes, J. Heliosch, F. Kneissl, L. Marco, A. Neumann, and H.-M. Seitz (Frankfurt), Chiranjeeb Sarkar (Edmonton), Jeff Harris (Glasgow), and Jock Robey (Kimberley). Jim Davidson and Andrew Rogers (Petra Diamonds) and Christo du Preez (Frontier Mining) gave permissions for the visits to the Bellsbank diamond mine. The

project was supported by the Deutsche Forschungsgemeinschaft (BR 1012/33-1 and BR 1012/37-1). Dave Green (University of Tasmania) gave decisive advice for the interpretation of the data and carefully read the manuscript. The comments and suggestions of L.A. Coogan and an anonymous reviewer on an earlier version greatly helped to improve the manuscript.

References

Aigner-Torres M, Blundy J, Ulmer P, Pettke T (2007) Laser ablation ICPMS study of trace element partitioning between plagioclase and basaltic melts: an experimental approach. Contrib Mineral Petrol 153:647–667

Allaz J, Maeder X, Vannay JC, Steck A (2005) Formation of aluminosilicate-bearing quartz veins in the Simano nappe (Central Alps): structural, thermobarometric and oxygen isotope constraints. Schweiz Miner Petrogr Mitt 85:191–214

Arevalo R, McDonough WF (2010) Chemical variations and regional diversity observed in MORB. Chem Geol 271:70–85

Aulbach S, Viljoen KS (2015) Eclogite xenoliths from the Lace kimberlite, Kaapvaal craton: from convecting mantle source to palaeo-ocean floor and back. Earth Planet Sci Lett 431:274–286

Bindeman IN, Kamenetsky VS, Palandri J, Vennemann T (2012) Hydrogen and oxygen isotope behaviors during variable degrees of upper mantle melting: example from the basaltic glasses from Macquarie Island. Chem Geol 310–311:126–136

Canil D (1999) Vanadium partitioning between orthopyroxene, spinel and silicate melt and the redox states of mantle source regions for primary magmas. Geochim Cosmochi Acta 63:557–572

Casey JF (1997) Comparison of major and trace element geochemistry of abyssal peridotites and mafic plutonic rocks with basalts from the MARK region of the mid-Atlantic ridge. In: Karson JA, Cannat M, Miller DJ, Elthon D (eds) Proceedings of the ocean drilling program, scientific results, vol 153, pp 181–241

Chapman DS, Pollack HN (1977) Regional geotherms and lithospheric thicknesses. Geology 5:265–268

Coleman RG, Lee DE, Beatty LB, Brannock WW (1965) Eclogites and eclogites: their differences and similarities. Geol Soc Am Bull 76:483–508

Coogan LA (1998) Magma plumbing beneath the Mid-Atlantic Ridge. Ph.D. thesis, University of Leicester

Coogan LA, Saunders AD, Kempton PD, Norry MJ (2000) Evidence from oceanic gabbros for porous melt migration within a crystal mush beneath the Mid-Atlantic Ridge. Geochem Geophys Geosyst 1:286

Creaser RA, Grütter H, Carlson J, Crawford B (2004) Macrocrystal phlogopite Rb–Sr dates for the Ekati property kimberlites, Slave Province, Canada: evidence for multiple intrusive episodes in the Paleocene and Eocene. Lithos 76:399–414

Drake MJ, Weill DF (1975) Partition of Sr, Ba, Ca, Y, Eu2+, Eu3+, and other REE between plagioclase feldspar and magmatic liquid: an experimental study. Geochim Cosmochim Acta 39:689–712

Eggins SM, Woodhead JD, Kinsley LPJ, Mortimer GE, Sylvester P, McCulloch MT, Hergt JM, Handler MR (1997) A simple method for the precise determination of >40 trace elements in geological sample by ICPMS using enriched isotope internal standardization. Chem Geol 134:311–326

Freise M, Holtz F, Nowak M, Scoates J, Strauss H (2009) Differentiation and crystallization conditions of basalts from the Kerguelen large igneous province: an experimental study. Contrib Miner Petrol 158:505–527

Gaetani GA, Grove TL (1997) Partitioning of moderately siderophile elements among olivine, silicate melt, and sulfide melt: constraints on core formation in the Earth and Mars. Geochim Cosmochim Acta 61(9):1829–1846

Gonzaga RG, Menzies MA, Thirlwall MF, Jacob DE, LeRoex A (2010) Eclogites and garnet pyroxenites: problems resolving provenance using Lu–Hf, Sm–Nd and Rb–Sr isotope systems. J Petrol 51:513–535

Gréau Y, Huang J-X, Griffin WL, Renac C, Alard O, O'Reilly SY (2011) Type I eclogites from Roberts Victor kimberlites: products of extensive mantle metasomatism. Geochim Cosmochim Acta 75:6927–6954

Green TH (1967) An experimental investigation of sub-solidus assemblages formed at high pressure in high-alumina basalt, kyanite eclogite and grospydite compositions. Contrib Miner Petrol 16:84–114

Green DH (2015) Experimental petrology of peridotites, including effects of water and carbon on melting in the Earth's upper mantle. Phys Chem Miner 42(2):95–122

Green DH, Ringwood AE (1967) The genesis of basaltic magmas. Contrib Miner Petrol 15:103–190

Green TH, Blundy JD, Adam J, Yaxley GM (2000) SIMS determination of trace element partition coefficients between garnet, clinopyroxene and hydrous basaltic liquids at 2–7.5 GPa and 1080–1200°C. Lithos 53:165–187

Heaman LM, Creaser RA, Cookenboo HO, Chacko T (2006) Multistage modification of the Northern slave mantle lithosphere: evidence from zircon-and diamond-bearing eclogite xenoliths entrained in Jericho kimberlite, Canada. J Petrol 47:821–858

Huang J-X, Griffin WL, Gréau Y, Pearson NJ, O'Reilly SY, Cliff J, Martin L (2014) Unmasking xenolithic eclogites: progressive metasomatism of a key Roberts Victor sample. Chem Geol 364:56–65

Jacob DE (2004) Nature and origin of eclogite xenoliths from kimberlites. Lithos 77:295–316

Jacob DE, Foley SF (1999) Evidence for Archean ocean crust with low high field strength element signature from diamondiferous eclogite xenoliths. Lithos 48:317–336

Jacob DE, Schmickler B, Schulze DJ (2003) Trace element geochemistry of coesite-bearing eclogites from the Roberts Victor kimberlite, Kaapvaal craton. Lithos 71:337–351

Jacob DE, Bizimis M, Salters VJM (2005) Lu/Hf and geochemical systematics of recycled ancient oceanic crust: evidence from Roberts Victor eclogites. Contrib Miner Petrol 148(6):707–720

Jagoutz E (1988) Nd and Sr systematics in an eclogite xenolith from Tanzania: evidence for frozen mineral equilibria in the continental lithosphere. Geochim Cosmochim Acta 52:1285–1293

Kasting JF, Eggler DH, Raeburn SP (1993) Mantle redox evolution and the oxidation state of the Archean atmosphere. J Geol 101:2 **(100th Anniversary Symposium: Evolution of the Earth's Surface 245–257)**

Knapp N, Woodland A, Klimm K (2013) Experimental constraints in the CMAS system on the Ca-Eskola content of eclogitic clinopyroxene. Eur J Mineral 25:579–596

Kornprobst J, Piboule M, Roden M, Tabit A (1989) Corundum-bearing garnet clinopyroxenites at Beni Bousera (Morocco): original plagioclase-rich gabbros recrystallized at depth within the mantle? J Petrol 31:717–746

Krogh EJ (1988) The garnet-clinopyroxene Fe-Mg geothermometer—a reinterpretation of existing experimental data. Contrib Miner Petrol 99:44–48

Kusakabe M, Maruyama S, Nakamura T, Yada T (2004) CO2 laser-Br F5 fluorination technique for analysis of three oxygen isotopes of rocks and minerals. J Mass Spectrom Soc Jpn 52:205–212

Laubier M, Grove T, Langmuir ChH (2014) Trace element mineral/melt partitioning for basaltic and basaltic andesitic melts: an experimental and laser ICP-MS study with application to the oxidation state of mantle source regions. Earth Planet Sci Lett 392:265–278

Lazarov M (2008) Archean to present day evolution of the lithospheric mantle beneath the Kaapvaal craton—processes recorded in subcalcic garnets, peridotites and polymict breccia. Ph.D. thesis Goethe-University Frankfurt. http://publikationen.ub.uni-frankfurt.de/files/6873/LazarovMarina.pdf

Lee C-TA, Leeman WP, Canil D, Li Z-XA (2005) Similar V/Sc systematics in MORB and Arc Basalts: implications for the oxygen fugacities of their mantle source regions. J Petrol 46(11):2313–2336

Li Z-XA, Lee C-TA (2004) The constancy of upper mantle fO2 through time inferred from V/Sc ratios in basalts. Earth Planet Sci Lett 228:483–493

Mallmann G, O'Neill HStC (2009) The crystal/melt partitioning of V during mantle melting as a function of oxygen fugacity compared with some other elements (Al, P, Ca, Sc, Ti, Cr, Fe, Ga, Y, Zr and Nb). J Petrol 50(9):1765–1794

Mattey D, Lowry D, MacPherson C (1994) Oxygen isotope composition of mantle peridotite. Earth Planet Sci Lett 128:231–241

McCulloch MT, Gregory RT, Wasserburg GJ, Taylor HP Jr (1981) Sm–Nd, Rb–Sr, and $^{18}O/^{16}O$ isotopic systematics in an oceanic crustal section: evidence from the Semail Ophiolite. J Geophys Res 86(B4):2721–2735

McDonough WF, Sun SS (1995) The composition of the Earth. Chem Geol 120:223–253

Menzies AH, Carlson RW, Shirey SB, Gurney JJ (2003) Re–Os systematics of diamond-bearing eclogites from the Newlands kimberlite. Lithos 71:323–336

Morishita T, Arai S (2001) Petrogenesis of corundum-bearing mafic rock in the Horoman Peridotite complex, Japan. J Petrol 42(7):1279–1299

Morishita T, Arai S, Green DH (2004) Possible non-melted remnants of subducted lithosphere: experimental and geochemical evidence from corundum-bearing mafic rocks in the Horoman peridotite complex, Japan. J Petrol 45(2):235–252

Muehlenbachs K, Clayton RN (1972) Oxygen isotope studies of fresh and weathered submarine basalts. Can J Earth Sci 9(2):172–184

Neal CR, Taylor AL, Davidson PJ, Holden P, Halliday NA, Nixon HP, Paces BJ, Clayton RN, Mayeda KT (1990) Eclogites with oceanic crustal and mantle signatures from the Bellsbank kimberlite, South Africa, part 2: Sr, Nd, and O isotope geochemistry. Earth Planet Sci Lett 99:362–379

Nixon PH, Chapman NA, Gurney JJ (1978) Pyrope-spinel (alkremite) xenoliths from kimberlite. Contrib Miner Petrol 65:341–346

Nowell GM, Pearson DG, Bell DR, Carlson RW, Smith CB, Kempton PD, Noble SR (2004) Hf isotope systematics of kimberlites and their megacrysts: new constraints on their source regions. J Petrol 45(8):1583–1612

Pearson DG, Nowell GM (2002) The continental lithospheric mantle: characteristics and significance as a mantle reservoir. Philos Trans R Soc Lond A 360:2383–2410

Pearson DG, Nowell GM (2004) Re-Os and Lu-Hf isotope constraints on the origin and age of pyroxenites from the Beni Bousera peridotite massif: implications for mixed peridotite-pyroxenite melting models. J Petrol Spec Ed Orog Lherzolites Mantle Process 54:439–455

Pearson DG, Snyder GA, Shirey SB, Taylor LA, Carlson RW, Sobolev NV (1995) Archaean Re–Os age for Siberian eclogites and constraints on Archaean tectonics. Nature 374:711–713

Perk NW, Coogan LA, Karson JA, Klein EM, Hanna HD (2007) Petrology and geochemistry of primitive lower oceanic crust from Pito Deep: implications for the accretion of the lower crust at the Southern East Pacific Rise. Contrib Miner Petrol 154:575–590

Pertermann M, Hirschmann MM, Hametner K, Guenther D, Schmidt M (2004) Experimental determination of trace element partitioning between garnet and silica-rich liquid during anhydrous partial melting of MORB-like eclogite. Geochem Geophys Geosyst 5:5

Presnall DC, Dixon SA, Dixon JR, O'Donnel TH, Brenner NL, Schrock RL, Dycus DW (1978) Liquidus phase pelations on the poin Diopside-Forsterite-Anorthite prom 1 atm to 20 kbar. Their bearing on the generation and crystallization of basaltic magma. Contrib Miner Petrol 66:203–220

Purwin H, Lauterbach S, Brey GP, Woodland AB, Kleebe H-J (2012) An experimental study of the Fe oxidation states in garnet and clinopyroxene as a function of temperature in the system CaO–FeO–Fe_2O_3–MgO–Al_2O_3–SiO_2: implications for garnet–clinopyroxene geothermometry. Contrib Miner Petrol 165:623–639

Råheim A, Green DH (1974) Experimental petrology of lunar highland basalt composition and applications to models for the lunar highland interior. J Geol 82:607–622

Rajamani V, Naldrett AJ (2006) Partitioning of Fe Co, Ni, and Cu between sulfide liquid and basaltic melts and the composition of Ni–Cu sulfide deposits. Econ Geol 73:82–93

Riches AJV, Ickert RB, Pearson DG, Stern RA, Jackson SE, Ishikawa A, Kjarsgaard BA, Gurney JJ (2015) In situ oxygen-isotope, major-, and trace-element constraints on the metasomatic modification and crustal origin of a diamondiferous eclogite from Roberts Victor, Kaapvaal Craton. Geochim Cosmochim Acta. doi:10.1016/j.gca.2015.11.028

Sarkar C, Heaman LM, Pearson DG (2015) Duration and periodicity of kimberlite volcanic activity in the Lac de Gras kimberlite field, Canada and some recommendations for kimberlite geochronology. Lithos 218:155–166

Schmidberger SS, Simonetti A, Heaman ML, Creaser AR, Whiteford S (2007) Lu–Hf, in situ Sr and Pb isotope and trace element systematics for mantle eclogites from the Diavik diamond mine: evidence for Paleoproterozoic subduction beneath the Slave craton, Canada. Earth Planet Sci Lett 254:55–68

Shu Q, Brey GP, Gerdes A, Hoefer HE (2014) Mantle eclogites and garnet pyroxenites—the meaning of two-point isochrons, Sm-Nd and Lu-Hf closure temperatures and the cooling of the subcratonic mantle. Earth Planet Sci Lett 389:143–154

Smith CB, Allsopp HL, Kramers JD, Hutchinson G, Roddick JC (1985) Emplacement ages of Jurassic-Cretaceous South African kimberlites by the Rb–Sr method on phlogopite and whole-rock samples. Trans Geol Soc S Afr 88:249–266

Taylor LA, Neal CR (1989) Eclogites with oceanic crustal and mantle signatures from the Bellsbank kimberlite, South Africa, part 1: mineralogy, petrography, and whole-rock chemistry. J Geol 97:551–567

Tepley FJ, Lundstrom CC, McDonough WF, Thomson A (2010) Trace element partitioning between high—an plagioclase and basaltic to basaltic andesite melt at 1 atmosphere pressure. Lithos 118:82–94

Valley JW, Kitchen N, Kohn MJ, Niendorf CR, Spicuzza MJ (1995) UWG-2, a garnet standard for oxygen isotope ratios: strategies for high precision and accuracy with laser heating. Geochim Cosmochim Acta 59:5223–5231